Ore Geology Reviews 104 (2019) 422–435

Contents lists available at ScienceDirect

Ore Geology Reviews

journal homepage: www.elsevier.com/locate/oregeorev

Sulphur and lead isotope geochemistry of sulphide minerals from the Zn-Pb-Cu-Ag-Au Lemarchant volcanogenic massive sulphide (VMS) deposit, Newfoundland, Canada

Shannon B. Gill[a,*], Stephen J. Piercey[a], Graham D. Layne[a], Glenn Piercey[b]

[a] Department of Earth Sciences, Memorial University of Newfoundland, St. John's, Newfoundland A1B 3X5, Canada
[b] CREAIT, Core Research Equipment and Instrument Training Network, Memorial University of Newfoundland, St. John's, Newfoundland A1B 3X5, Canada

ABSTRACT

The Lemarchant Zn-Pb-Cu-Ag-Au volcanogenic massive sulphide (VMS) deposit, in the Newfoundland Appalachians, Canada, is an important example of a precious metal-bearing VMS deposit. The deposit contains VMS- and sulphosalt-rich mineral assemblages, which are paragenetically distinct. Initial Zn-Pb-sulphosalt mineralization was deposited from low temperature (< 250 °C), weakly oxidized ($SO_4 \geq H_2S$), near-neutral fluids with high sulphur activity. Later Cu-rich, polymetallic mineralization was deposited from higher temperature (> 300 °C), less oxidized hydrothermal fluids with lower sulphur activity. *In situ* microanalyses of pyrite, chalcopyrite and galena yield a wide range of $\delta^{34}S$ values (−6.4 to +15.1‰). Sulphides from paragenetically early, lower temperature, Zn-Pb-sulphosalt assemblages have the lowest average $\delta^{34}S$ values (+4.6‰), whereas the highest $\delta^{34}S$ values occur in the late-stage, high-temperature, Cu-rich sulphide assemblages. Variability in $\delta^{34}S$ occurs in all styles of mineralization, and is consistent with S derived from thermochemical reduction of seawater sulphate, igneous leaching and, potentially, disproportionated magmatic SO_2. Although it is difficult to distinguish explicitly between leached igneous and magmatic sources of sulphur, mineralogical and geochemical data from Lemarchant suggest a possible contribution of magmatic SO_2 during the deposition of epithermal-style mineralization at the earlier stages of deposit formation.

Lead isotope compositions of galena show little variability with style of mineralization, suggesting similar Pb sources throughout ore deposition. Most Pb at Lemarchant is derived from underlying Neoproterozoic Sandy Brook group volcanic rocks, with potential input of juvenile Pb from the Lake Ambrose basaltic rocks of the Tally Pond group and/or from more juvenile Neoproterozoic basement rocks.

1. Introduction

Lead and sulphur isotopes are critical tools for understanding the sources of metals and sulphur in volcanogenic massive sulphide (VMS) and seafloor massive sulphide (SMS) deposits (Ohmoto, 1972; Sato et al., 1981; Janecky and Shanks, 1988; Huston, 1999; Tosdal et al., 1999; Shanks, 2001; Franklin et al., 2005; Seal, 2006). In ancient VMS deposits, circulating hydrothermal fluids transported metals and sulphur that were derived from the interaction of the fluids with a variety of rock types up to 2 km below the seafloor (Franklin et al., 2005; Galley et al., 2007; Gibson et al., 2007; Hannington and Monecke, 2009). Lead isotope compositions of sulphide minerals from both VMS and SMS deposits record the source(s) of metals and, in most published studies, the data indicate that lead is leached from underlying footwall or basement rocks (Stacey and Kramers, 1975; Zartman and Doe, 1981; Fouquet and Marcoux, 1995; Kramers and Tolstikhin, 1997; Tosdal et al., 1999; Franklin et al., 2005; Mortensen et al., 2006). In contrast, sulphur isotope systematics are much more complex due to the variety of sources and processes that can contribute to the S isotope composition of sulphide minerals (Jensen, 1967; Huston, 1999; Marini et al., 2011). The S isotope signature of sulphide minerals in most VMS deposits is attributed to seawater sulphate and/or sulphur leached from basement rocks (Janecky and Shanks, 1988; Ohmoto and Rye, 1979; Sakai et al., 1984; Halbach et al., 1989; Rye, 1993; Herzig et al., 1998; Shanks, 2001; Seal 2006). In rarer cases, S can be derived from bacteriogenic sources (Jensen, 1967; Janecky and Shanks, 1988; Huston, 1999; Shanks 2001) and/or magmatic fluids (de Ronde, 1995; Hannington et al., 1995; Herzig et al., 1998; de Ronde et al., 2005). The latter source has been inferred for certain ancient VMS environments, especially those with syngenetic precious metal enrichment (i.e., Herzig et al., 1993; Hannington et al., 1999a,b; Roth et al., 1999; Ulrich et al., 2002; Chiaradia et al., 2008). Additionally, isotopic compositions of sulphide minerals can change with fluid evolution during the formation of the deposit because S isotopes can be strongly fractionated by variation in certain physicochemical characteristics of the hydrothermal fluid, particularly those involving redox reactions that change the speciation of sulphur (e.g., Ohmoto, 1972; Ohmoto and Lasaga, 1982; Ohmoto and Goldhaber, 1997).

* Corresponding author.
E-mail address: shannon.gill@kinross.com (S.B. Gill).

https://doi.org/10.1016/j.oregeorev.2018.11.008
Received 20 May 2017; Received in revised form 5 November 2018; Accepted 10 November 2018
Available online 15 November 2018

Although radiogenic and stable isotope systematics in VMS systems are invaluable in understanding deposit genesis, only limited Pb and S isotope data are available for Appalachian VMS deposits (e.g., Swinden and Thorpe, 1984; Goodfellow and Peter, 1996; Pollock and Wilton, 2001; Pollock, 2004). There are even fewer *in situ* Pb and S isotope data available for Appalachian and global VMS deposits, and their application to understanding precious metal-enriched VMS deposits globally has not been fully tested.

The bimodal felsic Zn-Pb-Cu-Ag-Au Lemarchant VMS deposit in central Newfoundland comprises five distinct styles of mineralization, which were deposited in three sequential stages from an evolving hydrothermal system (Gill et al., 2015; Gill et al., 2016). The Lemarchant deposit provides an excellent opportunity to investigate Pb and S isotope evolution in a type example of precious metal bearing Appalachian VMS deposit. In this paper, paragenetically controlled *in situ* Pb and S isotope data for major sulphide minerals in the Lemarchant deposit are presented, along with interpretations of the source(s) of metals and sulphur in the deposit and the hydrothermal fluid evolution during sulphide mineralization. These data also provide key insights into potential sources of Pb and S in similar precious metal enriched VMS deposits in the Appalachians and globally.

2. Regional geological setting

The Lemarchant deposit is located in the Dunnage Zone of the Newfoundland Appalachians, which is composed of nascent to mature volcanic arc, arc-rift and back arc basin sequences (Swinden et al., 1988; Rogers et al., 2006; McNicoll et al., 2010; Piercey and Hinchey, 2012). The Red Indian Line divides the Dunnage Zone into the western peri-Laurentian Notre Dame subzone and eastern peri-Gondwanan Exploits subzone, representing opposing sides of the Iapetus suture zone (Fig. 1, inset; Williams et al., 1988; Evans and Kean, 2002; Rogers et al., 2006; McNicoll et al., 2010). The volcanic and sedimentary rocks within the Exploits subzone were accreted to the Ganderian subcontinent during the mid-Ordovician Penobscot Orogeny, and subsequently accreted to composite Laurentia along the Red Indian Line during the Late Ordovician (Rogers and van Staal, 2002; Rogers et al., 2006; van Staal and Barr, 2012; Piercey et al., 2014). The Lemarchant deposit is hosted in the Victoria Lake supergroup of the Exploits subzone, which consists of six discrete volcanic assemblages (e.g., Rogers and van Staal, 2002; Rogers et al., 2006; Zagorevski et al., 2007) and is underlain by Neoproterozoic metavolcanic and metaplutonic basement rocks (Sandy Brook group and Crippleback/Valentine Lake intrusive suites, respectively; Rogers et al., 2006; McNicoll et al., 2010).

The oldest and lowermost volcanic assemblage in the Victoria Lake supergroup is the Cambrian Tally Pond group (~513–509 Ma; Pollock, 2004; McNicoll et al., 2010), which forms part of the eastern margin of the Exploits subzone (Fig. 1). The Tally Pond group is informally divided into the Bindons Pond and Lake Ambrose formations (Rogers et al., 2006; ~Boundary Brook formation and Lake Ambrose basalts, respectively, of Dunning et al., 1991). The Bindons Pond formation is composed of transitional to calc-alkaline island arc volcanic rocks that are dominated by rhyolite to dacite flows, volcaniclastic rocks and carbonaceous shales (Evans and Kean, 2002; Rogers et al., 2006; Copeland et al., 2008; Piercey and Hinchey, 2012; Piercey et al., 2014). The Lake Ambrose formation is interlayered with the Bindons Pond formation, and is composed predominantly of mafic, sub-alkalic to depleted tholeiitic island arc volcanic rocks (Evans and Kean, 2002; Rogers et al., 2006; Copeland et al., 2008; Piercey and Hinchey, 2012). The Bindons Pond formation is host to the majority of massive sulphide mineralization in the Tally Pond group, including the past-producing Duck Pond and Boundary VMS deposits, and the Lemarchant VMS deposit (McNicoll et al., 2010; Piercey and Hinchey, 2012). The Lemarchant deposit occurs at a contact between the Bindons Pond felsic volcanic rocks and overlying Lake Ambrose mafic volcanic rocks, and was formed during a hiatus in effusive volcanism in an extensional arc-rift setting (Evans and Kean, 2002; Rogers and van Staal, 2002; Rogers et al., 2006; van Staal and Barr, 2012; Piercey et al., 2014).

3. Deposit geology

The Lemarchant deposit is hosted in a bimodal felsic volcanic assemblage, and can be broadly divided into a semi-conformable massive to semi-massive sulphide zone ("stratiform zone") and a discordant stringer sulphide zone ("stringer zone"). The barite-rich stratiform zone strikes 350 m northwest, is generally ≤20 m thick, and occurs at the contact between the felsic footwall and the mafic hanging wall (Fig. 2A). A thin, pyritic mudstone layer occurs at the footwall-hanging wall contact immediately above the stratiform zone (Fig. 2B). The stringer zone is situated below the stratiform zone within the footwall felsic rocks. Stringer sulphide mineralization does not extend far below the stratiform zone and is abruptly truncated, possibly indicating removal of a lower stringer zone during Silurian-Devonian thrust faulting (see below; Dunning et al., 1991; Squires and Moore, 2004; Rogers et al., 2006). A portion of the deposit (the "Northwest zone") is also displaced 200 m to the northwest, > 100 m below the main mineralized zone (Fig. 2), and is mineralogically and geochemically similar to the main mineralized zone (Gill et al., 2016).

The footwall rocks are composed of aphyric rhyolite flows/domes, breccia, lapilli tuffs and tuff breccia, polylithic lapilli tuffs and minor tuffs (Squires and Moore, 2004; Copeland et al., 2008). Massive and interstitial granular barite occurs at the top of the footwall and is variably replaced by sulphide mineralization. The thin, pyritic and variably graphitic mudstone layer capping the footwall contains minor sulphide stringers and is interpreted to be, in part, an exhalative sedimentary rock (Copeland et al., 2008; Lode et al., 2015). The pyritic mudstone is intercalated with the overlying mafic hanging wall proximal to mineralization, and is considered to have formed prior to and during mineralization at Lemarchant (Lode et al., 2016a,b, 2015). Hanging wall rocks are composed of massive basalt to basaltic andesite, vesicular pillow basalt and hyaloclastite breccia, and are variably magnetic (Squires and Moore, 2004; Copeland et al., 2008; Piercey and Hinchey, 2012). Three types of intrusions crosscut the mineralized lithologies at Lemarchant, including two types of mafic dykes and a less common type of felsic dyke: (1) light brown to green, pyroxene phyric synvolcanic mafic dykes, commonly with peperitic and vesicular margins (Pollock, 2004; Squires and Moore, 2004; Copeland et al., 2008); (2) grey-green medium-grained diabase to gabbroic dykes with sharp contacts; and (3) pink to white, aphyric to lesser quartz phyric felsic dykes.

The felsic volcanic footwall is quartz and sericite altered with lesser albite, proximal to the overlying stratiform barite horizon, and chlorite. However, sections of chlorite-dominated alteration occur locally in the stringer zone, and devitrified glass fragments in brecciated rhyolite are strongly chlorite altered (Copeland et al., 2008; Gill and Piercey, 2014; Gill et al., 2015). The mafic hanging wall is weakly altered to quartz, chlorite and minor epidote, with pyrite and rare cross-cutting pyrrhotite, arsenopyrite and chalcopyrite mineralization (Copeland et al., 2008; Fraser et al., 2012). Fuchsite occurs in synvolcanic dykes. Late carbonate alteration is abundant, in the form of quartz-carbonate stringers that crosscut all lithologies at Lemarchant; carbonate bleaching at mafic dyke contacts; and trace ankerite disseminated throughout the mafic lithologies.

Repetition of the bimodal volcanic stratigraphy in the Lemarchant deposit (Fig. 2B) suggests thrust imbricated stacking of the footwall host rock, particularly along the Lemarchant Fault, and the deposit has been disrupted by a number of (possibly reactivated?) upright normal faults (Squires and Moore, 2004; Copeland et al., 2008; Fraser et al., 2012). Low-grade greenschist metamorphism accompanied deformation during Silurian-Devonian tectonic activity (Dunning et al., 1991; Squires and Moore, 2004; Rogers et al., 2006). Although the deposit has been variably deformed, there is only minor local remobilization of

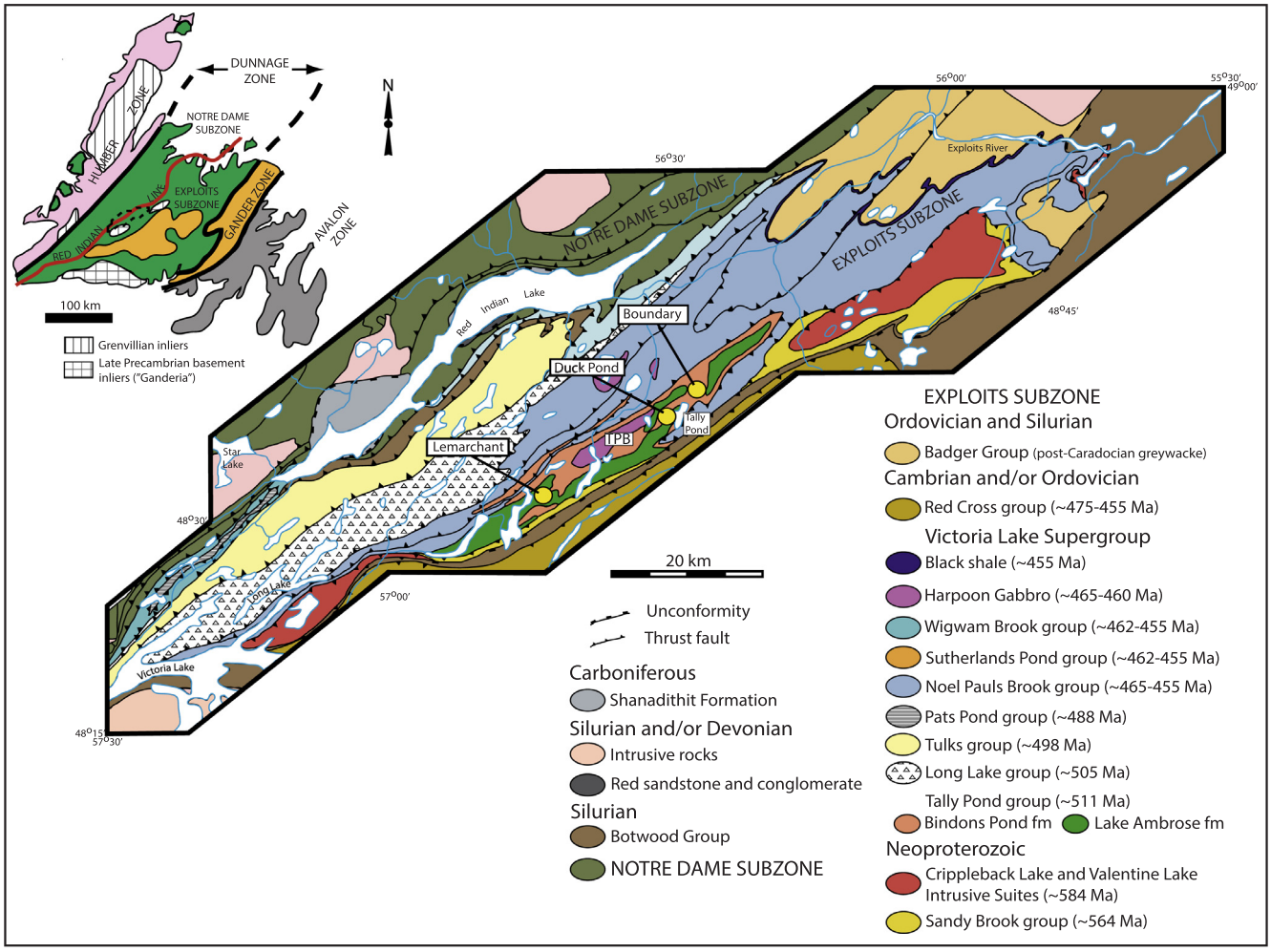

Fig. 1. Geological map of the Victoria Lake supergroup in the Exploits subzone, Newfoundland. Locations of the Lemarchant, Duck Pond and Boundary VMS deposits within the Tally Pond belt (TPB) are indicated. Inset map of tectonostratigraphic sequences comprising Newfoundland (modified after Rogers et al., 2006; McNicoll et al., 2010; Piercey and Hinchey, 2012).

sulphide mineralization, with excellent preservation of sulphide mineral textures in the stratiform and stringer zones.

4. Sulphide mineralization

The sulphide mineralogy at Lemarchant is dominated by sphalerite and pyrite, with lesser galena, chalcopyrite, tetrahedrite-tennantite, and bornite (Fig. 3). Minor minerals include pyrrhotite, arsenopyrite, marcasite, and visible electrum. Trace minerals are colusite-germanocolusite, stromeyerite, covellite, polybasite, miargyrite, and bournonite, with unidentified silver tellurides, nickel sulphides, Cu-Sb-Ag- and Cu-V-bearing sulphosalts. Gold occurs primarily as electrum at Lemarchant; however, laser ablation inductively coupled plasma mass spectrometry (LA-ICP-MS) analyses reveal Au is also resident in pyrite, either as lattice substitutions or as micro-inclusions of Au (Gill et al., 2016). Silver is hosted in the tetrahedrite-tennantite series of minerals such as Ag-tetrahedrite and tetrahedrite, in electrum, and in the Ag-bearing sulphosalts; trace Ag is also present in galena (Gill et al., 2016). Gold contents in electrum are higher in the centre of the deposit, whereas Ag-rich electrum and Ag-bearing minerals are more abundant at the outer edges of the deposit (Gill et al., 2016).

Sulphide mineralization at Lemarchant is concentrated in the barite-rich stratiform zone, with lesser sulphides in the underlying stringer zone. Sulphide mineral associations and textures are used to define five mineral assemblage types (Gill et al., 2015; Gill et al., 2016): Type 1 semi-massive granular barite-pale sphalerite-colloform pyrite-galena (± chalcopyrite-tetrahedrite-tennantite) (Fig. 3A and 4); Type 2A bornite-galena-chalcopyrite (± stromeyerite-covellite-Ni-sulphide) stringers (Fig. 3B and 4); Type 2B disseminated tetrahedrite-tennantite-galena-bladed barite-white sphalerite-recrystallized pyrite (± electrum-colusite-germanocolusite-polybasite-miargyrite-bournonite-Ag-tellurides) (Fig. 3B-D and 4); Type 3 massive dark sphalerite-subhedral to euhedral pyrite-galena-chalcopyrite(± pyrrhotite-arsenopyrite) (Figs. 3E-F and 4); and Type 4 chalcopyrite-euhedral pyrite (± orange sphalerite-galena) stringers (Figs. 3G-H and 4).

In the stratiform zone, the type 1 assemblage is intergrown with massive barite mineralization, and is partially replaced by type 2A stringers and infilled by the type 2B assemblage. Type 3 mineralization overlies and partially replaces the upper portion of the stratiform zone mineralization. The stringer zone lies stratigraphically below the stratiform zone, is composed of type 4 stringers, and is devoid of barite.

The five mineral assemblages were deposited in three paragenetic stages, each with distinct pyrite textures (Fig. 4; Gill et al., 2016). In the first stage of paragenesis, barite and low-Fe pale sphalerite type 1 mineralization was deposited with fine-grained colloform pyrite from a low temperature (150–275 °C), likely weakly oxidized ($SO_4 \geq H_2S$) and mildly acidic hydrothermal fluid (Gill et al., 2016). The second stage encompassed partial replacement and infill of type 1 mineralization by the intermediate sulfidation, sulphosalt-rich type 2A and type 2B mineral assemblages, and resulted in recrystallization of type 1 pyrite to

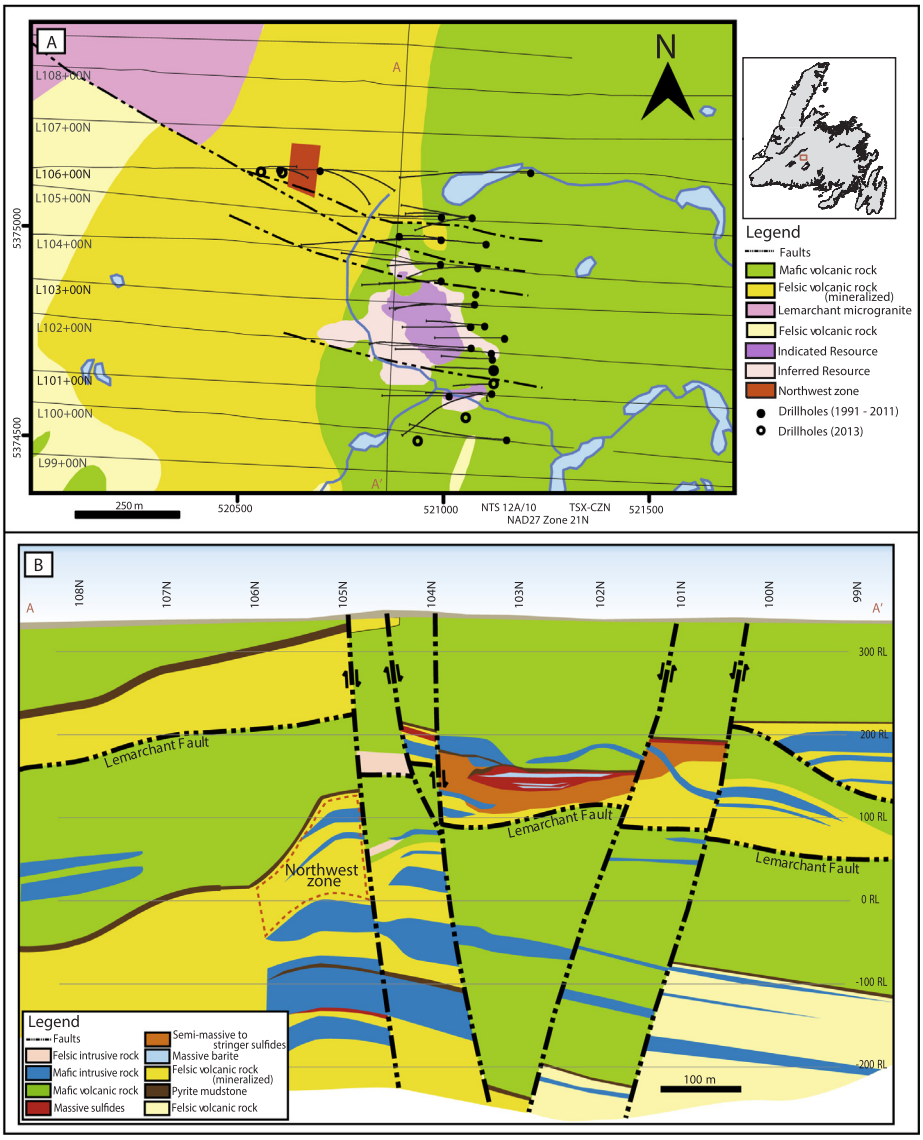

Fig. 2. Geology of the Lemarchant deposit. A) Schematic geological map with superimposed northing grid; inferred and indicated resources, Northwest zone and logged drill hole locations projected to surface, and long section A-A' indicated. B) Long section along A-A' through main mineralized zone; depths at given relative survey levels. Plan view and cross section modified from Fraser et al. (2012).

form rounded to subhedral, fine- to medium-sized grains of pyrite. Replacement and minor zone refinement of the stratiform zone by barite-poor, high-Fe dark sphalerite type 3 mineralization, and formation of the basal stringer zone with chalcopyrite dominated type 4 sulphides occurred during the third paragenetic stage. The mineral assemblages deposited during this final stage of mineralization are consistent with formation from a higher temperature (> 300 °C), intermediate state ($SO_4 \approx H_2S$) hydrothermal fluid (Gill et al., 2016).

5. Isotope geochemistry of sulphide minerals

5.1. Analytical methods

Samples were selected from five drill holes to represent the five types of mineral assemblages described above. Offcuts corresponding to eight thin section samples that were previously analyzed by scanning electron microscopy, electron microprobe analysis and LA-ICP-MS (Gill et al., 2016), were epoxy mounted in 25.4 mm diameter Al rings. The mounts were polished using standard lapidary procedures and sputter coated with Au (~300 Å). *In situ* isotope microanalyses were performed using a Cameca IMS 4f™ secondary ion mass spectrometer (SIMS) at the MAF-IIC facility, Memorial University of Newfoundland. Procedures for analyses of Pb and S isotopes are outlined below; supplementary methods are provided in Appendix A, and in Brueckner et al. (2015) and Cloutier et al. (2015) for Pb and S isotopes, respectively.

Lead isotope analyses were performed exclusively on galena, which is effectively uranium-free and thus does not contain any U-decay related radiogenic Pb (i.e., galena is representative of original hydrothermal Pb sources). Where possible, galena was selected to represent each of the five types of mineralization, but some bias was introduced due to the relative abundance of mineral grains ≥ 25 μm in diameter) in the different assemblages. Three grains were selected per sample, and two spots were analyzed per grain to monitor possible zonal variation in Pb isotope values. An O^- primary ion beam with a 14–16 nA current at a nominal 10 keV potential was focused into a 15–20 μm diameter spot. The spot to be analyzed was first rastered for 120 s over 25 μm^2 and then pre-sputtered for 75 s over 10 μm^2 prior to measurement to eliminate potential surface contamination. The analytical method consisted of 15 cycles of peak switching and counting between the different Pb isotopes (1.0 s on background, 8.0 s on $^{204}Pb^+$, and 4.0 s on

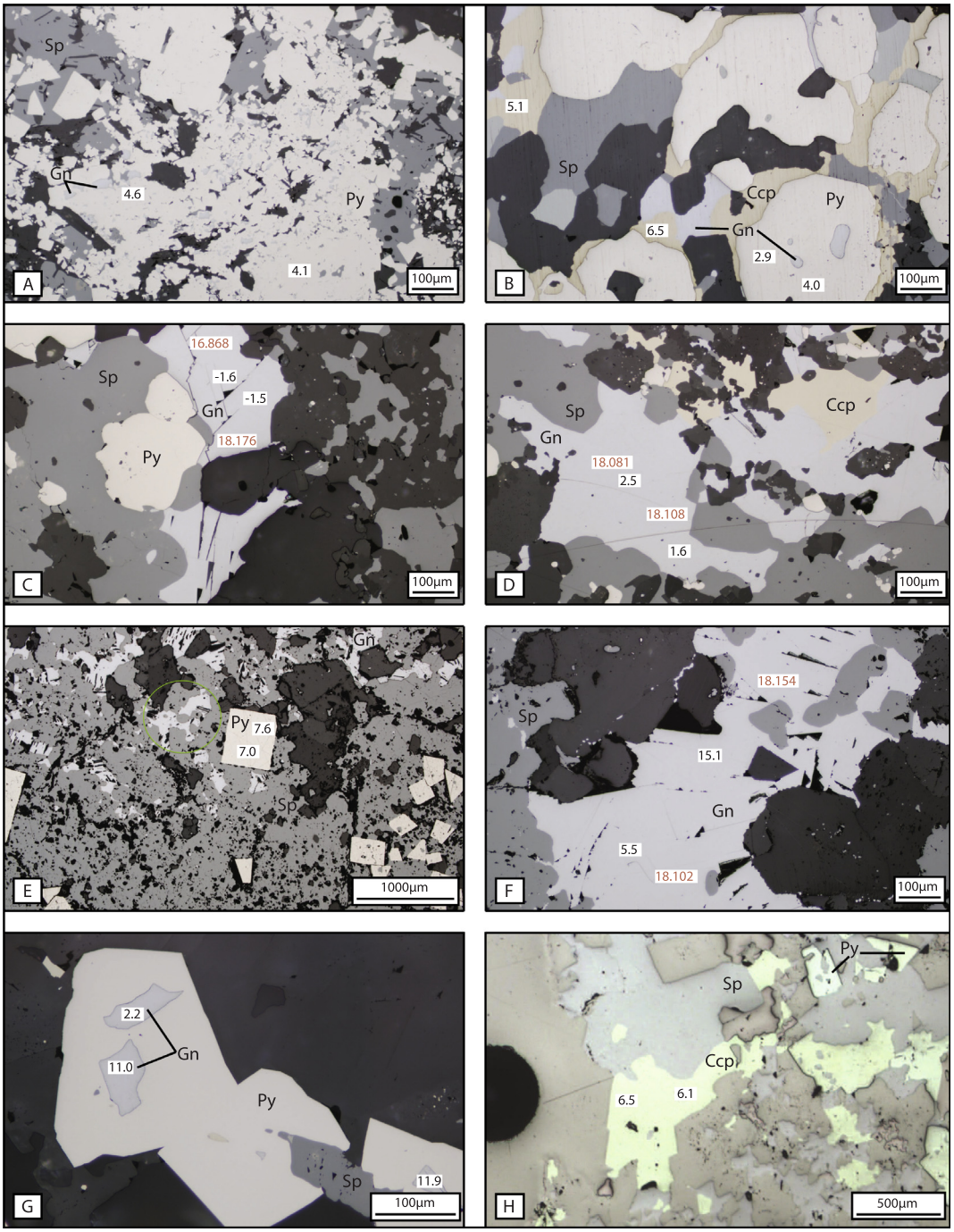

Fig. 3. Photomicrograph compilation of representative mineral textures in pyrite, galena and chalcopyrite in the type mineral assemblages at Lemarchant. Sulfur-isotope values (per mil; black) and Pb-isotope ratios ($^{206}Pb/^{204}Pb$; red) are shown at spot analysis locations. A) Variably recrystallized colloform pyrite representing stage 1 deposition (Sample CNF29960 in drill hole LM11-59 at 216 m depth). B) Rounded atoll pyrite and interstitial type 2A chalcopyrite from stage 2 deposition (CNF29957 in LM11-63 at 210.8 m). C) Fractured, pitted type 2A galena from stage 2 deposition (CNF14259 in LM07-14 at 204.4 m). D) Amorphous type 2B galena from stage 2 deposition (CNF29962 in LM11-59 at 225.9 m). E) Euhedral pyrite representing stage 3 deposition (CNF14291 in LM11-65 at 159.3 m). F) Pitted type 3 galena from stage 3 deposition (CNF29959 in LM11-59 at 207.7 m). G) Type 4 galena inclusions from stage 3 deposition in recrystallized atoll pyrite (CNF29972 in LM11-59 at 251.2 m). H) Type 4 chalcopyrite stringers from stage 3 mineralization (CNF29972 in LM11-59 at 251.2 m). Abbreviations as follows: Sp = sphalerite; Py = pyrite; Ccp = chalcopyrite; Gn = galena. (For interpretation of the references to colour in this figure legend, the reader is referred to the web version of this article.)

$^{206}Pb^+$, $^{207}Pb^+$ and $^{208}Pb^+$, with 0.4 s waiting time between each isotope to allow for magnet settling (0.5 s before background)). Total analysis time for a single spot was 9 min. Pb isotope analyses in samples of galena were corrected for instrumental mass fractionation (IMF) by comparison to replicate run measurements of F19 galena reference material. Average IMF for the data presented in Table 1 was 0.45%/Da. Detailed analytical procedures followed those in Lode et al. (2016b). A secondary reference material, JMBH (galena), was analyzed periodically to monitor accuracy and reproducibility. External precision determined from replicate standard analyses of JMBH galena reference material was typically better than ± 0.1–0.15% for these same ratios. Internal precision of individual spot measurements of $^{206}Pb/^{204}Pb$,

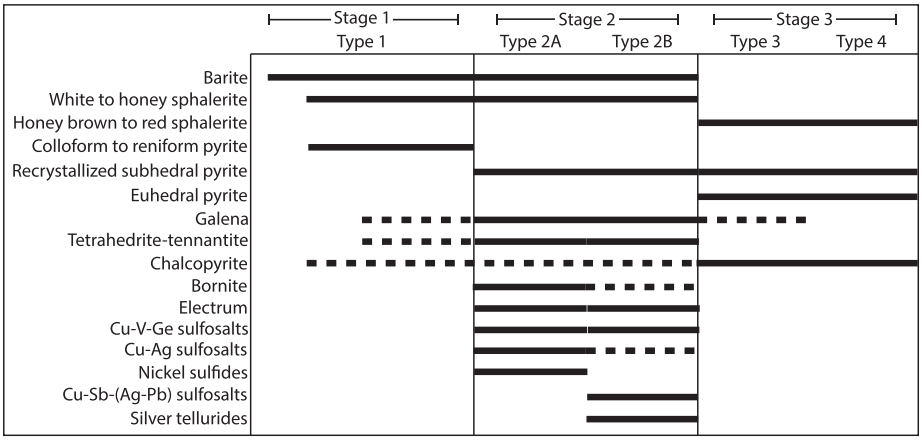

Fig. 4. Simplified paragenetic scheme highlighting the three main stages of mineral deposition at the Lemarchant deposit and the five type mineral assemblages.

Table 1
Lead-isotope ratios, internal precision (1σ (%)), covariation (rho) and μ-values (after Stacey and Kramers, 1975) of analyzed galena samples at Lemarchant. Atypical outlier values of dataset (three samples in CNF14259) are italicized.

Drill Hole	Depth (m)	Sample	$^{206/204}$Pb	1σ (%)	$^{207/204}$Pb	1σ (%)	$^{208/204}$Pb	1σ (%)	rho 7/6	rho 8/6	μ
Type 2A: Bornite-galena-chalcopyrite stringers in massive barite-sphalerite-pyrite-galena											
LM07-14	*185.3*	*CNF14259 Pb1*	*17.393*	*0.247*	*15.632*	*0.572*	*38.003*	*0.624*	*0.433*	*0.397*	*10.19*
LM07-14	*185.3*	*CNF14259 Pb2*	*17.932*	*0.430*	*15.639*	*0.596*	*38.016*	*0.607*	*0.721*	*0.708*	*9.99*
LM07-14	185.3	CNF14259 Pb3	18.176	0.062	15.642	0.086	38.002	0.081	0.724	0.763	9.94
LM07-14	*185.3*	*CNF14259 Pb4*	*16.868*	*0.525*	*15.624*	*0.866*	*37.842*	*0.745*	*0.607*	*0.705*	*10.49*
LM07-14	185.3	CNF14259 Pb5	18.092	0.105	15.557	0.133	37.638	0.150	0.791	0.699	9.58
LM07-14	185.3	CNF14259 Pb6	18.211	0.117	15.677	0.143	38.078	0.143	0.821	0.820	10.08
LM11-63	194.1	CNF29957 Pb1	18.098	0.123	15.586	0.132	37.733	0.137	0.926	0.896	9.72
LM11-63	194.1	CNF29957 Pb2	18.181	0.064	15.669	0.074	38.091	0.087	0.872	0.742	10.05
LM11-63	194.1	CNF29957 Pb3	18.138	0.108	15.599	0.113	37.830	0.114	0.961	0.950	9.76
LM11-63	194.1	CNF29957 Pb4	18.137	0.084	15.605	0.113	37.872	0.098	0.743	0.862	9.79
LM11-63	194.1	CNF29957 Pb5	18.134	0.124	15.572	0.136	37.740	0.157	0.914	0.794	9.63
LM11-63	194.1	CNF29957 Pb6	18.129	0.114	15.581	0.128	37.708	0.140	0.894	0.818	9.68
Type 2B: galena-tetrahedrite-barite-pyrite-sphalerite-gold in massive barite-sphalerite-pyrite-galena											
LM11-65	155.2	CNF14291 Pb1	18.110	0.131	15.572	0.145	37.881	0.157	0.907	0.836	9.69
LM11-65	155.2	CNF14291 Pb2	18.100	0.089	15.489	0.106	37.349	0.118	0.833	0.749	9.27
LM11-65	155.2	CNF14291 Pb3	18.043	0.086	15.476	0.093	37.487	0.096	0.925	0.898	9.22
LM11-65	155.2	CNF14291 Pb4	18.061	0.160	15.570	0.170	37.879	0.185	0.945	0.866	9.65
LM11-65	155.2	CNF14291 Pb5	18.103	0.066	15.690	0.123	38.076	0.127	0.542	0.523	10.20
LM11-65	155.2	CNF14291 Pb6	18.076	0.087	15.624	0.126	37.910	0.112	0.693	0.776	9.88
LM11-59	194.7	CNF29962 Pb1	18.069	0.100	15.516	0.119	37.648	0.146	0.840	0.681	9.39
LM11-59	194.7	CNF29962 Pb2	18.116	0.055	15.530	0.066	37.629	0.075	0.839	0.733	9.44
LM11-59	194.7	CNF29962 Pb3	18.081	0.114	15.496	0.118	37.586	0.127	0.961	0.897	9.30
LM11-59	194.7	CNF29962 Pb4	18.108	0.116	15.524	0.125	37.628	0.123	0.922	0.943	9.42
LM11-59	194.7	CNF29962 Pb5	18.062	0.133	15.492	0.162	37.584	0.172	0.820	0.774	9.30
LM11-59	194.7	CNF29962 Pb6	18.143	0.066	15.578	0.079	37.799	0.089	0.832	0.742	9.66
LM08-19	88.5	CNF29986 Pb1	18.140	0.074	15.595	0.089	37.876	0.091	0.832	0.816	9.74
LM08-19	88.5	CNF29986 Pb2	18.171	0.123	15.535	0.149	37.650	0.143	0.828	0.858	9.46
LM08-19	88.5	CNF29986 Pb3	18.120	0.091	15.569	0.105	37.836	0.123	0.871	0.740	9.62
LM08-19	88.5	CNF29986 Pb4	18.127	0.077	15.568	0.089	37.780	0.098	0.867	0.781	9.62
LM08-19	88.5	CNF29986 Pb5	18.127	0.138	15.554	0.155	37.697	0.173	0.889	0.796	9.55
LM08-19	88.5	CNF29986 Pb6	18.063	0.143	15.515	0.157	37.698	0.158	0.914	0.907	9.39
Type 3: Massive sphalerite-pyrite-chalcopyrite-galena											
LM11-59	179.0	CNF29959 Pb1	18.102	0.100	15.552	0.110	37.726	0.112	0.906	0.889	9.55
LM11-59	179.0	CNF29959 Pb2	18.154	0.089	15.630	0.108	38.002	0.108	0.820	0.817	9.88
LM11-59	179.0	CNF29959 Pb3	18.180	0.127	15.629	0.133	37.932	0.138	0.957	0.921	9.89
LM11-59	179.0	CNF29959 Pb4	18.177	0.100	15.625	0.110	37.898	0.107	0.906	0.935	9.87
LM11-59	179.0	CNF29959 Pb5	18.164	0.105	15.604	0.125	37.994	0.152	0.839	0.688	9.78
LM11-59	179.0	CNF29959 Pb6	18.155	0.099	15.635	0.113	38.027	0.150	0.873	0.661	9.91
LM11-59	186.1	CNF29960 Pb1	18.032	0.104	15.449	0.138	37.476	0.143	0.757	0.729	9.26
LM11-59	186.1	CNF29960 Pb2	18.128	0.143	15.578	0.155	37.831	0.159	0.918	0.896	9.66
LM11-59	186.1	CNF29960 Pb3	18.109	0.083	15.528	0.111	37.665	0.106	0.746	0.779	9.44
LM11-59	186.1	CNF29960 Pb4	18.097	0.087	15.522	0.113	37.624	0.113	0.769	0.768	9.41
LM11-59	186.1	CNF29960 Pb5	18.088	0.092	15.539	0.129	37.671	0.143	0.714	0.647	9.30

^{207}Pb/^{204}Pb, and ^{208}Pb/^{204}Pb ranged between 0.05–0.15%, 0.05–0.15%, and 0.075–0.175%, respectively. Explicit numbers for internal precision are included in Table 1.

Sulphur isotope analyses were performed on pyrite, chalcopyrite and galena grains ≥25 μm in diameter. Where possible, sulphide minerals were selected to represent each of the five mineral assemblages but, as for Pb isotope microanalysis of galena, some bias was introduced due to relative abundance of mineral grains ≥25 μm in each

assemblage. Three grains were selected per sample, and two spots were analyzed per grain to monitor possible zonal variation in S isotope values. A Cs^+ primary ion beam with a 0.6–0.8 nA current for pyrite and chalcopyrite, and a 0.9–1.0 nA current for galena, at a nominal 10 keV potential was focused into a 5–15 μm diameter spot. The spot to be analyzed was first rastered for 120 s over 25 μm^2, and then pre-sputtered for 200 s over 10 μm^2. The analytical method consisted of 80 cycles of peak switching and counting between the different S isotopes (0.5 s on background, 2.0 s on $^{32}S^-$ and 6.0 s on $^{34}S^-$, with 0.25 s waiting time between each peak to allow for magnet settling). Analysis time for a single spot was approximately 15 min. Correction for instrumental mass fractionation was performed using standard reference materials UL9B (pyrite; $\delta^{34}S$: 15.8‰ VCDT), Norilsk (chalcopyrite; $\delta^{34}S$: 8.3‰ VCDT) and HT10 (galena; $\delta^{34}S$: 14.2‰ VCDT). Results are expressed as $\delta^{34}S$ relative to Vienna Canyon Diablo troilite (VCDT). Internal precision (standard error of the mean) on measured $\delta^{34}S$ values of the standards were routinely better than ± 0.3‰ (1σ). External reproducibility of replicate standard analyses was routinely better than ± 0.35–0.45‰ (1σ). Further details are provided in Brueckner et al. (2015) and Cloutier et al. (2015).

5.2. Lead isotope results

A total of 42 *in situ* SIMS analyses were conducted on galena from the stratiform zone of the Lemarchant deposit (Table 1). Overall, lead isotope ratios are clustered between 18.03 and 18.21 (average 18.12 ± 0.10), 15.45 to 15.69 (average 15.57 ± 0.12) and 37.35 to 38.09 (average 37.78 ± 0.13) for $^{206}Pb/^{204}Pb$, $^{207}Pb/^{204}Pb$ and $^{208}Pb/^{204}Pb$, respectively (Table 1; Fig. 5). Three outliers exist in the Lemarchant data that deviate from the overall $^{206}Pb/^{204}Pb$ trend, and these are discussed below. Galena in type 1 and type 4 sulphides were not analyzed due to their extremely small grain sizes; however, Pb isotope ratios from the type 2A, type 2B and type 3 assemblages have significant overlap and are considered to originate from the same source(s) (Fig. 5).

Certain features are evident when Pb isotope ratios are plotted in uranogenic ($^{207}Pb/^{204}Pb$ vs. $^{206}Pb/^{204}Pb$) and thorogenic ($^{208}Pb/^{204}Pb$ vs. $^{206}Pb/^{204}Pb$) space and compared to the Pb isotope growth curves for known reservoirs from Kramers and Tolstikhin (1997) (Fig. 5). The Lemarchant data have $^{206}Pb/^{204}Pb$ ratios that are very close to expected values for young upper crust at ~500 Ma, but with varying $^{208}Pb/^{204}Pb$ and $^{207}Pb/^{204}Pb$ (Fig. 5). With the exception of the three anomalous values, galena has Stacey and Kramers (1975) calculated μ values that range from 9.22 to 10.20 (Table 1). The average μ value for Lemarchant (9.63) is similar to the μ value for young upper crust at 500 Ma (μ = 9.66; Kramers and Tolstikhin, 1997). However, the variance from the average value and the variation in $^{208}Pb/^{204}Pb$ and $^{207}Pb/^{204}Pb$ requires mixed contributions from less evolved (lower μ) and, to a lesser extent, more evolved (higher μ) sources (Fig. 5). The isochrons generated from these data are not included here, as they yield model ages (Stacey and Kramers, 1975) that are not meaningful in mixed Pb isotope-source systems such as Lemarchant.

Outliers in Lemarchant Pb isotope data deviate only from the $^{206}Pb/^{204}Pb$ analyses at 17.393, 17.932 and 16.868 in sample CNF14259, but are within the range of the values for $^{207}Pb/^{204}Pb$ and $^{208}Pb/^{204}Pb$ analyses (Table 1). Galena from sample CNF14259 in the type 2A assemblage are overall extensively pitted (i.e., Fig. 3C) and have an excursively large $^{206}Pb/^{204}Pb$ error relative to other samples (Table 1), so these outliers are most likely attributed to the uneven crystal surface of the galena, which harboured exotic Pb from surface contamination that was difficult to remove by pre-sputtering.

5.3. Sulphur isotope results

Results for *in situ* S isotope analyses for pyrite, galena and chalcopyrite are presented in Table 2. The overall range of $\delta^{34}S$ values in Lemarchant sulphide minerals is between −6.4 and +15.1‰ (average +5.0 ± 3.3‰ (1σ), n = 119).

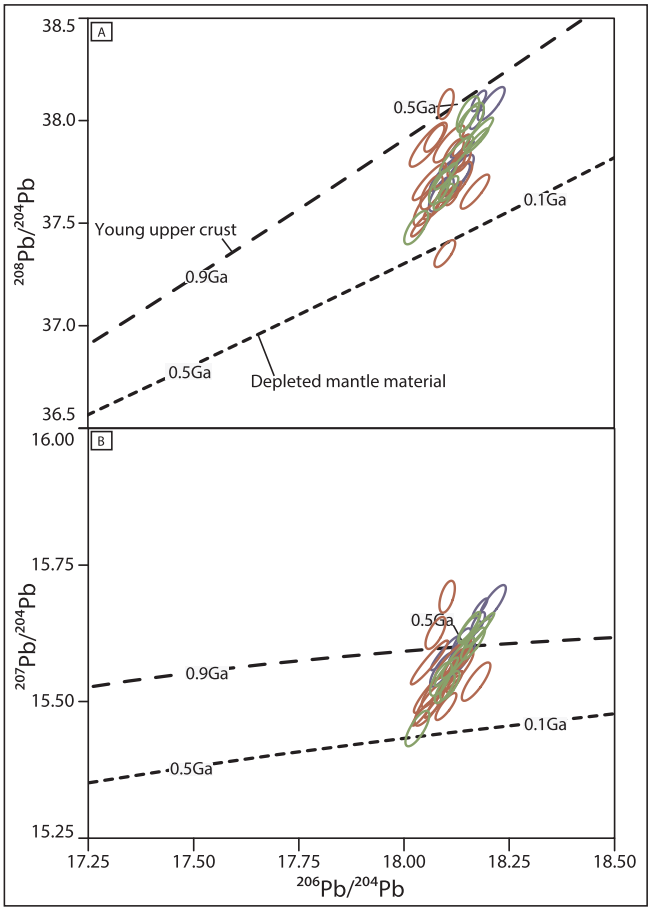

Fig. 5. Plots of Pb-isotope variation in galena in the Lemarchant deposit for A) $^{208}Pb/^{204}Pb$ vs. $^{206}Pb/^{204}Pb$ (thorogenic lead) and B) $^{207}Pb/^{204}Pb$ vs. $^{206}Pb/^{204}Pb$ (uranogenic lead). Error ellipses represent internal precision of 1σ (%). Growth curves for young upper crust (long dashed line) and depleted mantle material (short dashed line) after Kramers and Tolstikhin (1997). Three outliers in sample CNF14259 are not included in diagram.

The $\delta^{34}S$ of type 1 fine-grained, colloform to recrystallized pyrite ranges from +0.3 to +4.9‰ (average +3.6 ± 1.7‰, n = 8); the average value is slightly lower than the average for the entire deposit (Table 2; Fig. 6). The $\delta^{34}S$ of type 2A galena ranges from −1.6 to +4.8‰ (average +1.4 ± 2.2‰, n = 12), with one outlier at +11.8‰ associated with a pitted grain. The $\delta^{34}S$ of type 2A chalcopyrite ranges from + 5.2 to +6.2‰ (average +5.8 ± 0.5‰, n = 6). The $\delta^{34}S$ of type 2B rounded, recrystallized pyrite and chalcopyrite $\delta^{34}S$ ranges from +2.9 to +10.6‰ (average +5.9 ± 1.7‰, n = 28) and +3.0 to +5.0‰ (average +4.1 ± 0.7‰, n = 12), respectively. The $\delta^{34}S$ observed for type 2B galena is highly variable, ranging from −1.7 to +13.0‰ (average +4.4 ± 4.0‰, n = 12).

Type 3 galena has a very wide range of $\delta^{34}S$, from −6.4 to +15.1‰ (average +4.5 ± 6.6‰, n = 12); the highest values (+13.2 and +15.1‰; Table 2) occur in discrete grains and are not caused by pitted surfaces (i.e., Fig. 3F). Euhedral pyrite in the type 3 assemblage has $\delta^{34}S$ ranging from +5.4 to +8.3‰ (average +6.9 ± 0.8‰, n = 12).

The type 4 mineral assemblage displays the highest mean $\delta^{34}S$ in the Lemarchant deposit (Fig. 6), largely because of the wide range of $\delta^{34}S$ for galena (+2.2 and +12.0‰; average +7.2 ± 4.2‰, n = 5). Chalcopyrite $\delta^{34}S$ for type 4 are much less variable, ranging from +5.8 to + 6.5‰ (average +6.2 ± 0.3‰, n = 6).

Table 2
Sulfur-isotope values (per mil VCDT) of pyrite, chalcopyrite and galena from each type mineral assemblage at Lemarchant. Standard error of the mean (SEM) included to 1σ.

Drill hole	Depth (m)	Sample	Mineral	$\delta^{34}S$	SEM (1σ)
Type 1: Massive barite-semi-massive sphalerite-pyrite-galena					
LM11-59	186.1	CNF29960 py1	Pyrite	0.3	0.3
LM11-59	186.1	CNF29960 py2	Pyrite	1.7	0.2
LM11-59	186.1	CNF29960 py3	Pyrite	4.9	0.2
LM11-59	186.1	CNF29960 py4	Pyrite	4.4	0.2
LM11-59	186.1	CNF29960 py5	Pyrite	4.9	0.3
LM11-59	186.1	CNF29960 py6	Pyrite	4.2	0.2
LM11-59	186.1	CNF29960 py7	Pyrite	4.1	0.2
LM11-59	186.1	CNF29960 py8	Pyrite	4.6	0.2
Type 2A: Bornite-galena-chalcopyrite stringers					
LM11-63	194.1	CNF29957 gn1	Galena	4.7	0.3
LM11-63	194.1	CNF29957 gn2	Galena	−0.2	0.3
LM11-63	194.1	CNF29957 gn3	Galena	4.1	0.3
LM11-63	194.1	CNF29957 gn4	Galena	3.7	0.3
LM11-63	194.1	CNF29957 gn5	Galena	2.3	0.3
LM11-63	194.1	CNF29957 gn6	Galena	2.5	0.3
LM07-14	185.3	CNF14259 gn1	Galena	−1.6	0.6
LM07-14	185.3	CNF14259 gn2	Galena	−1.5	0.3
LM07-14	185.3	CNF14259 gn3	Galena	11.8	0.3
LM07-14	185.3	CNF14259 gn4	Galena	0.4	0.2
LM07-14	185.3	CNF14259 gn5	Galena	1.1	0.3
LM07-14	185.3	CNF14259 gn6	Galena	−0.2	0.3
LM11-63	194.1	CNF29957 ccp1	Chalcopyrite	5.8	0.3
LM11-63	194.1	CNF29957 ccp2	Chalcopyrite	6.5	0.5
LM11-63	194.1	CNF29957 ccp3	Chalcopyrite	5.4	0.8
LM11-63	194.1	CNF29957 ccp4	Chalcopyrite	6.0	0.6
LM11-63	194.1	CNF29957 ccp5	Chalcopyrite	5.1	0.8
LM11-63	194.1	CNF29957 ccp6	Chalcopyrite	6.2	0.6
Type 2B: Galena-tetrahedrite-barite-pyrite-sphalerite-gold					
LM11-63	194.1	CNF29957 py1	Pyrite	4.2	0.3
LM11-63	194.1	CNF29957 py2	Pyrite	3.8	0.2
LM11-63	194.1	CNF29957 py3	Pyrite	3.9	0.2
LM11-63	194.1	CNF29957 py4	Pyrite	4.1	0.3
LM11-63	194.1	CNF29957 py5	Pyrite	2.9	0.2
LM11-63	194.1	CNF29957 py6	Pyrite	4.0	0.2
LM08-19	88.5	CNF29986 py1	Pyrite	5.5	0.3
LM08-19	88.5	CNF29986 py2	Pyrite	6.5	0.2
LM08-19	88.5	CNF29986 py3	Pyrite	5.6	0.3
LM08-19	88.5	CNF29986 py4	Pyrite	6.5	0.3
LM08-19	88.5	CNF29986 py5	Pyrite	5.4	0.3
LM08-19	88.5	CNF29986 py6	Pyrite	7.4	0.2
LM11-59	194.7	CNF29962 py1	Pyrite	6.4	0.3
LM11-59	194.7	CNF29962 py2	Pyrite	6.6	0.2
LM11-59	194.7	CNF29962 py3	Pyrite	6.4	0.3
LM11-59	194.7	CNF29962 py4	Pyrite	6.1	0.3
LM11-59	194.7	CNF29962 py5	Pyrite	6.8	0.3
LM11-59	194.7	CNF29962 py6	Pyrite	6.8	0.3
LM07-14	185.3	CNF14259 py1	Pyrite	6.1	0.3
LM07-14	185.3	CNF14259 py2	Pyrite	6.3	0.2
LM07-14	185.3	CNF14259 py3	Pyrite	4.8	0.3
LM07-14	185.3	CNF14259 py4	Pyrite	5.8	0.2
LM07-14	185.3	CNF14259 py5	Pyrite	5.1	0.6
LM07-14	185.3	CNF14259 py6	Pyrite	4.8	0.3
LM11-59	179.0	CNF29959 py1	Pyrite	10.6	0.3
LM11-59	179.0	CNF29959 py2	Pyrite	9.5	0.2
LM11-59	179.0	CNF29959 py3	Pyrite	6.2	0.5
LM11-59	179.0	CNF29959 py4	Pyrite	7.6	0.2
LM11-65	155.2	CNF14291 gn1	Galena	6.8	0.3
LM11-65	155.2	CNF14291 gn2	Galena	4.9	0.3
LM11-65	155.2	CNF14291 gn3	Galena	7.9	0.3
LM11-65	155.2	CNF14291 gn4	Galena	5.5	0.2
LM11-65	155.2	CNF14291 gn5	Galena	12.6	0.3
LM11-65	155.2	CNF14291 gn6	Galena	13.0	0.2
LM08-19	88.5	CNF29986 gn1	Galena	−1.7	0.4
LM08-19	88.5	CNF29986 gn2	Galena	0.0	0.4
LM08-19	88.5	CNF29986 gn3	Galena	1.6	0.3
LM08-19	88.5	CNF29986 gn4	Galena	7.4	0.2
LM08-19	88.5	CNF29986 gn5	Galena	2.5	0.3
LM08-19	88.5	CNF29986 gn6	Galena	1.5	0.2
LM11-59	194.7	CNF29962 gn1	Galena	5.3	0.2
LM11-59	194.7	CNF29962 gn2	Galena	3.0	0.3
LM11-59	194.7	CNF29962 gn3	Galena	2.5	0.2
LM11-59	194.7	CNF29962 gn4	Galena	1.6	0.3
LM11-59	194.7	CNF29962 gn5	Galena	0.3	0.4
LM11-59	194.7	CNF29962 gn6	Galena	5.2	0.4
LM11-59	194.7	CNF29962 ccp1	Chalcopyrite	4.3	0.4
LM11-59	194.7	CNF29962 ccp2	Chalcopyrite	3.8	0.3
LM11-59	194.7	CNF29962 ccp3	Chalcopyrite	3.5	0.4
LM11-59	194.7	CNF29962 ccp4	Chalcopyrite	2.9	0.4
LM11-59	194.7	CNF29962 ccp5	Chalcopyrite	3.3	0.4
LM11-59	194.7	CNF29962 ccp6	Chalcopyrite	3.9	0.3
LM08-19	88.5	CNF29986 Ccp1	Chalcopyrite	4.8	0.5
LM08-19	88.5	CNF29986 Ccp2	Chalcopyrite	4.6	0.3
LM08-19	88.5	CNF29986 Ccp3	Chalcopyrite	4.5	0.5
LM08-19	88.5	CNF29986 Ccp4	Chalcopyrite	3.9	0.4
LM08-19	88.5	CNF29986 Ccp5	Chalcopyrite	5.1	0.4
LM08-19	88.5	CNF29986 Ccp6	Chalcopyrite	5.0	0.4
Type 3: Massive sphalerite-pyrite-chalcopyrite-galena					
LM11-65	155.2	CNF14291 py1	Pyrite	8.3	0.2
LM11-65	155.2	CNF14291 py2	Pyrite	7.4	0.2
LM11-65	155.2	CNF14291 py3	Pyrite	7.6	0.3
LM11-65	155.2	CNF14291 py4	Pyrite	7.0	0.2
LM11-65	155.2	CNF14291 py5	Pyrite	6.9	0.2
LM11-65	155.2	CNF14291 py6	Pyrite	7.5	0.3
LM11-59	216.5	CNF29972 py1	Pyrite	6.8	0.4
LM11-59	216.5	CNF29972 py2	Pyrite	6.7	0.2
LM11-59	216.5	CNF29972 py3	Pyrite	6.2	0.3
LM11-59	216.5	CNF29972 py4	Pyrite	6.7	0.2
LM11-59	216.5	CNF29972 py5	Pyrite	6.2	0.4
LM11-59	216.5	CNF29972 py6	Pyrite	5.4	0.2
LM11-59	186.1	CNF29960 gn1	Galena	4.2	0.3
LM11-59	186.1	CNF29960 gn2	Galena	3.0	0.3
LM11-59	186.1	CNF29960 gn3	Galena	-6.0	0.2
LM11-59	186.1	CNF29960 gn4	Galena	2.5	0.3
LM11-59	186.1	CNF29960 gn5	Galena	0.4	0.2
LM11-59	186.1	CNF29960 gn6	Galena	−6.4	0.3
LM11-59	179.0	CNF29959 gn1	Galena	8.8	0.4
LM11-59	179.0	CNF29959 gn2	Galena	7.6	0.4
LM11-59	179.0	CNF29959 gn3	Galena	6.6	0.3
LM11-59	179.0	CNF29959 gn4	Galena	13.2	0.3
LM11-59	179.0	CNF29959 gn5	Galena	5.5	0.3
LM11-59	179.0	CNF29959 gn6	Galena	15.1	0.4
Type 4: Chalcopyrite-pyrite ± sphalerite-galena stringers					
LM11-59	216.5	CNF29972 gn1	Galena	5.3	0.3
LM11-59	216.5	CNF29972 gn2	Galena	5.4	0.6
LM11-59	216.5	CNF29972 gn3	Galena	2.2	0.3
LM11-59	216.5	CNF29972 gn4	Galena	11.0	0.3
LM11-59	216.5	CNF29972 gn5	Galena	11.9	0.4
LM11-59	216.5	CNF29972 ccp1	Chalcopyrite	5.8	0.5
LM11-59	216.5	CNF29972 ccp2	Chalcopyrite	6.2	0.3
LM11-59	216.5	CNF29972 ccp3	Chalcopyrite	6.4	0.3
LM11-59	216.5	CNF29972 ccp4	Chalcopyrite	6.5	0.3
LM11-59	216.5	CNF29972 ccp5	Chalcopyrite	6.5	0.3
LM11-59	216.5	CNF29972 ccp6	Chalcopyrite	6.1	0.3

6. Discussion

6.1. Source(s) of Pb

Lead isotopes provide a proxy for the potential sources of some metals in VMS deposits. The Lemarchant Pb isotope data form an elongate cluster (Fig. 5) that closely resembles the steep trend of whole rock Pb isotope data previously published for other deposits in the Tally Pond group (Swinden and Thorpe, 1984; Cumming and Krstic, 1987; Winter and Wilton, 2000; Pollock and Wilton, 2001). It also overlaps bulk analysis-type Pb data published for other peri-Gondwanan deposits in the Appalachians (Fig. 8; Swinden and Thorpe, 1984; Pollock and Wilton, 2001; Pollock, 2004).

The clustering of Pb isotopic data proximal to the young upper crust curve (Fig. 5; Kramers and Tolstikhin, 1997) is consistent with the regional geology and tectonics of the Tally Pond group. The volcanic

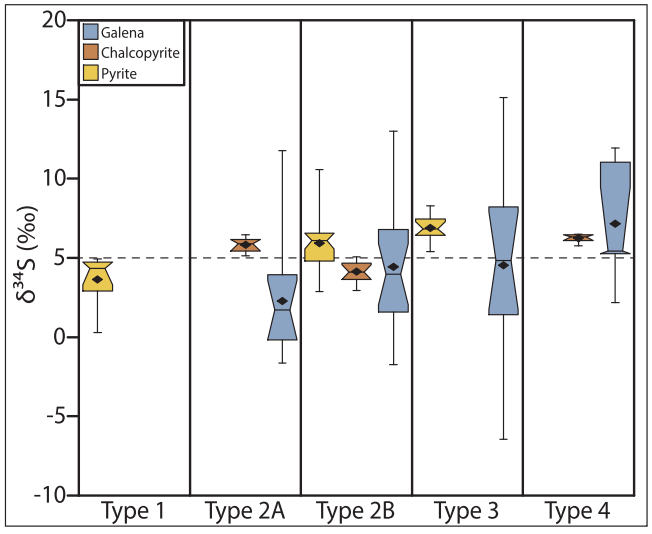

Fig. 6. Notched box and whisker plot of $\delta^{34}S$ variation in pyrite, chalcopyrite and galena from each type mineral assemblage. Data are significantly different (95% confidence level) if notches about medians do not overlap (after McGill et al., 1978). Mean values for each type sulfide are indicated as black diamonds. Dashed line indicates mean value for entire dataset.

rocks of the Tally Pond group are underlain by ~564 Ma Neoproterozoic volcanic and intrusive rocks that include a bimodal volcanic assemblage (the Sandy Brook group) with continental arc signatures and $\varepsilon Nd_t < 0$ (Rogers et al., 2006; McNicoll et al., 2010; Lode et al., 2017). The Tally Pond volcanic rocks, including the host rocks to mineralization in the Tally Pond group, were erupted through the Neoproterozoic basement rock, and contain inherited zircons and εNd_t values consistent with crustal inheritance (Rogers et al., 2006; McNicoll et al., 2010; Lode et al., 2017). The Pb signature of the Lemarchant deposit likely originates predominantly from Pb derived from the relatively young, Neoproterozoic basement rock immediately underlying the Tally Pond group.

Although there is a predominant upper crustal component contributing to the Pb isotopic array of the Lemarchant deposit, a number of samples (Table 1) have lower μ values than the ~500 Ma value for young upper crust (μ = 9.66; Kramers and Tolstikhin, 1997). These lower μ values require that a more juvenile crustal component also contributed to the Pb isotope array at Lemarchant, and the aforementioned regional framework accommodates this as well. Abundant mafic rocks in the underlying Neoproterozoic Sandy Brook group, and basalts to basaltic andesites in the lowermost unit of the Tally Pond group (the Lake Ambrose formation; Evans and Kean, 2002; Rogers et al., 2006; Lode et al., 2017) have arc tholeiitic to calc-alkalic affinities and $\varepsilon Nd_t > 0$. Even the felsic rocks within the Tally Pond group have $\varepsilon Nd_t > 0$, implying that they contain some juvenile material (Rogers et al., 2006; McNicoll et al., 2010; Lode et al., 2017). Although there are no published Pb isotopic data for the mafic lithologies of the Sandy Brook group or the Tally Pond group, it is reasonable to suggest that these lithologies have juvenile Pb isotopic signatures with μ values lower than young upper crust given their εNd_t signatures. Lead leached from these mafic sources would account for the juvenile component apparent in the Lemarchant Pb isotope array.

On a regional scale, Pb isotope data at Lemarchant correlate well with those of the Dunnage Zone. Lemarchant and other massive sulphide deposits in the Exploits subzone are enriched in radiogenic Pb relative to the massive sulphide deposits in the Notre Dame subzone to the west (Fig. 8; Swinden and Thorpe, 1984; Pollock and Wilton, 2001; Pollock, 2004; Goodfellow, 2007). This pattern is consistent with the derivation of Pb from different source regions, on opposing sides of the Iapetus Ocean (Swinden and Thorpe, 1984; Rogers and van Staal, 2002; Zagorevski et al., 2007; van Staal and Barr, 2012). The slightly more radiogenic Pb signatures of Exploits subzone deposits (i.e., Tally Pond and Tulks volcanic groups, and Wild Bight Group; Fig. 8) have been attributed to the proximity of these deposits to the sedimentary rocks of the early Paleozoic Ganderian passive margin (i.e., Gander Group and Spruce Brook Formation; Swinden and Thorpe, 1984; Pollock, 2004; van Staal and Barr, 2012) and, more generally, the Gondwanan realm (Pollock and Wilton, 2001) from which the older, more radiogenic Pb was likely sourced. Results from the Lemarchant deposit are also consistent with Pb derived from this Ganderian basement rock (Fig. 8).

Despite the common homogenization of Pb isotopes in some VMS hydrothermal systems from district- to camp-scale, particularly in the Precambrian (e.g., Thorpe, 1999; Mortensen et al., 2006), the non-homogeneity of Pb isotopes at Lemarchant is consistent with regional geological data and is similar to previous TIMS (i.e., conventional) Pb isotopic data on galena (e.g., Pollock and Wilton, 2001), suggesting that the distribution is not an analytical artifact (Fig. 8). Further, the much finer spatial resolution of SIMS microanalysis (10 s of μm versus 100 s–1000 s of μm for conventional analysis) better maps the extremes of these dispersions at Lemarchant by resolving much smaller scale variations recorded as individual galena crystals grew. This imples that the Pb isotope distribution at Lemarchant is real, consistent with existing data and regional geology, and reflects derivation of Pb from at least two different sources (i.e., evolved and juvenile Pb) before reaching the site of mineralization.

6.2. Source(s) of S

The sources of reduced sulphur (H_2S) in VMS deposits are primarily: 1) reduced seawater sulphate (SO_4^{2-}); 2) sulphide leached from igneous basement rock; and 3) disproportionated exsolved magmatic SO_2 (Jensen, 1967; Ohmoto and Rye, 1979; Janecky and Shanks, 1988; Huston, 1999; Shanks, 2001; Seal, 2006). Seawater SO_4^{2-} may be reduced to H_2S either organically (bacterial sulphate reduction – BSR) or inorganically (thermochemical sulphate reduction – TSR) (Huston, 1999; Shanks, 2001; Seal, 2006). In closed or partially closed systems, reduction of seawater sulphate through bacterial activity can result in a very wide range of $\delta^{34}S$ values (Shanks, 2001; Seal, 2006). However, in relatively open systems, such as that inferred for the barite-rich Lemarchant deposit, the source of SO_4^{2-} is continually replenished and preferential reduction of the isotopically light sulphate ($^{32}SO_4^{2-}$) results in the formation of sulphide minerals with extremely negative $\delta^{34}S$ values (i.e., ≤ −30‰; Ohmoto and Rye, 1979; Goodfellow and Peter, 1996; Seal, 2006). Although the initial stages of deposition at Lemarchant were relatively low temperature (and permissive of bacterial activity; Ohmoto and Rye, 1979; Goodfellow and Peter, 1996), the lightest $\delta^{34}S$ observed is not less than 0‰ for pyrite and chalcopyrite, and not less than −7‰ for galena; nor was there textural evidence of extensive bacterial activity, such as framboidal pyrite within the deposit. This suggests that BSR did not contribute significantly to the sulphur budget of the massive or stringer sulphide mineralization at Lemarchant.

Thermochemical sulphate reduction in circulating hydrothermal seawater generally occurs at temperatures > 200 °C, upon interaction of the hot fluid with reduced iron (or a similar reductant) in the host or basement rocks (Ohmoto and Rye, 1979; Shanks, 2001; Seal, 2006). Reduced sulphur produced by TSR of seawater can display a wide range of positive $\delta^{34}S$ values, which are partly dependent on the original $\delta^{34}S$ value of the seawater sulphate (Sakai and Dickson, 1978; Ohmoto and Rye, 1979; Seal, 2006). The $\delta^{34}S$ values of sulphide minerals formed from TSR-derived H_2S are therefore possible to predict based on estimates of original seawater $\delta^{34}S$, temperature and the proportion of original seawater sulphate reservoir already reduced (Eq. (6.2.1) after Ohmoto and Rye, 1979; Ohmoto and Goldhaber, 1997):

$$1000ln\alpha_{(H_2S-SO_4)} = A * \frac{10^6}{T^2} + B * \frac{10^3}{T} + C = \delta^{34}S_{H_2S} - \delta^{34}S_{SO_4} \quad (6.2.1)$$

where $\alpha_{(H2S-SO4)}$ is the fractionation factor (difference between sulphide and sulphate isotope ratios during TSR); T is the temperature in Kelvin; A, B, and C are constants (A = -5.26, and B and C are = 0 in this equation; Ohmoto and Goldhaber, 1997); $\delta^{34}S_{SO4}$ is the sulphur isotope composition of seawater sulphate; and $\delta^{34}S_{H2S}$ is the sulphur isotope composition of H_2S generated by TSR. Thermochemical sulfate reduction was calculated at the likeliest lower (200 °C) and upper (300 °C) temperatures of Lemarchant mineralization based on the presence of Zn-Pb-rich vs. Cu-rich mineral assemblages, respectively, within the range of temperatures that support thermochemical sulphate reduction (Ohmoto and Rye, 1979; Seyfried and Bischoff, 1981; Shanks, 2001; Seal, 2006). The $\delta^{34}S$ of H_2S generated by TSR was calculated using Eq. (6.2.2):

$$\delta^{34}S_{H_2S} = \delta^{34}S_{SO_4(parent,t)} + 1000\left(\alpha_{(H_2S-SO_4)} - 1\right) \quad (6.2.2)$$

and relates the sulphur isotope compositions of H_2S derived from seawater sulphate to the Rayleigh distillation equation (Eq. (6.2.3); Shanks et al., 1995):

$$\delta^{34}S_{SO_4(parent,t)} = (\delta^{34}S_{SO_4(parent,t=0)} + 1000) * f^{(\alpha_{(H_2S-SO_4)}-1)} - 1000 \quad (6.2.3)$$

Equation (6.2.3) describes $\delta^{34}S_{SO4\ (parent,\ t)}$ as the $\delta^{34}S$ value of SO_4^{2-} at some time relative to the original composition of seawater sulphate ($\delta^{34}S_{SO4\ (parent,\ t=0)}$), and as a function of the proportion of seawater sulphate reduced to H_2S (f). Given the abundance of barite at Lemarchant, it is highly probable that the system was open to the seawater sulphate reservoir and that there was continuous recharge of sulphate during TSR (i.e., $f = 1$). Additionally, it was assumed that seawater sulphate had a $\delta^{34}S_{Cambrian}$ ~35‰ (Claypool et al., 1980; Shanks, 2001; Canfield, 2004; Kampschulte and Strauss, 2004; Paytan and Gray, 2012), and that the sulphide minerals crystallized between 200 and 300 °C.

Considering only TSR, the $\delta^{34}S$ values predicted for phases crystallizing between 200 and 300 °C range from 13 to 20‰ for pyrite, 14 to 20‰ for galena and 14 to 19‰ for chalcopyrite (Appendix B). These values are much higher than the majority of samples examined from Lemarchant, and suggest that TSR alone cannot explain the sulphur isotope data. Mixing of TSR-derived H_2S in the hydrothermal fluid with additional source(s) of reduced sulphur with lower $\delta^{34}S$ values would have been required to produce the range of $\delta^{34}S$ observed in the Lemarchant sulphides.

Potential sources for lower $\delta^{34}S$ sulphur are igneous and magmatic sulphur. Igneous basement rock and magmatic fluids have similar sulphur isotope signatures (Huston, 1999; Shanks, 2001; Franklin et al., 2005; Seal, 2006). In particular, primitive igneous materials such as mid-ocean ridge basalts (MORB) and ocean island basalts (OIB) have $\delta^{34}S$ close to the average isotopic value of magmatic fluids (i.e., ~0‰; Ohmoto and Rye, 1979; Sakai et al., 1984; Seal, 2006), and continental and island arc basalts are shown to have similar isotopic values with $\delta^{34}S$ ~0‰ (Ueda and Sakai, 1984). Tholeiitic basalts with island arc-affinities are present in both the host rock sequence to the Lemarchant deposit (i.e., Lake Ambrose formation; Copeland et al., 2008; McNicoll et al., 2010) and in the basement rock underlying the deposit (i.e., the Sandy Brook group; Rogers et al., 2006; McNicoll et al., 2010). Additionally, the intrusive igneous rocks below the deposit (Lemarchant microgranite) and the Neoproterozoic basement rock (Crippleback Lake intrusive suite) likely have magmatic $\delta^{34}S$ values of ~0 ± 3‰ (e.g., Ohmoto and Goldhaber, 1997; Seal, 2006). However, although a leached igneous sulphur source may explain some $\delta^{34}S$ values near 0‰ in the Lemarchant dataset, it might not explain the $\delta^{34}S$ < 0‰ present in sulphides deposited during the earlier stages of mineralization (Figs. 6 and 7).

The 0‰ to slightly negative $\delta^{34}S$ values may be derived from magmatic fluids contributing light sulphur (Ohmoto and Rye, 1979; Franklin et al., 2005; Seal, 2006). At temperatures above 300 °C the dominant sulphur species in magmatic fluids is SO_2, but with cooling, the magmatic SO_2 disproportionates to form H_2S and H_2SO_4 (Ohmoto, 1972; Ohmoto and Lasaga, 1982; Herzig et al., 1998; Rye, 1993; Seal, 2006). This reaction is accompanied by a large isotopic fractionation, which produces sulphide minerals with negative $\delta^{34}S$ relative to associated sulphate minerals (Rye, 1993; Huston et al., 2011). Furthermore, early-stage mineral assemblages at Lemarchant contain sulphosalt minerals (i.e., bornite, tetrahedrite, colusite, covellite, electrum; Gill et al., 2015; Gill et al., 2016) that are referred to as the "epithermal suite" of minerals in VMS deposits (e.g., Sillitoe et al., 1996; Hannington et al., 1999a,b; Dube et al., 2007; Hannington and Monecke, 2009). The sulphide and sulphosalt minerals associated with stages 1 and 2 of mineralization also contain enrichments in "epithermal suite" trace elements and Au (As, Bi, Co, Cr, In, Mo, Ni, Sb, Se, Te; Gill et al., 2016). These assemblages are also associated with bladed barite rimmed by sulphosalt minerals (e.g., Lajoie, 2017; Lajoie et al., submitted for publication) that are texturally similar to bladed minerals in boiling zones of epithermal systems (e.g., White and Hedenquist, 1990) and to those found in modern magmatic fluid influenced seafloor hydrothermal systems (e.g., de Ronde et al., 2005). Thus, the lighter $\delta^{34}S$ values associated with the sulphosalt-rich and epithermal suite element-bearing mineral assemblages in the Lemarchant dataset are similar to other precious metal bearing VMS and SMS deposits worldwide, and suggest a potential magmatic input into the Lemarchant VMS system (e.g., Fig. 9; Lau Basin, Herzig et al., 1998; Eskay Creek, Sherlock et al., 1999; Mt. Morgan, Ulrich et al., 2002).

It is suggested that the deposition of early stage, sulphosalt-rich mineral assemblages at Lemarchant was a result of fluid boiling where the fluid had a magmatic component (Gill et al., 2015; Gill et al., 2016). Boiling would have provoked disproportionation of magmatic SO_2 in the hydrothermal fluid and resulted in light $\delta^{34}S$ signatures in associated sulphide minerals (Ohmoto, 1972; Rye, 1993; Hannington et al., 1999a,b; Huston, 2000; Seal, 2006; Hannington and Monecke, 2009; Huston et al., 2011). There is evidence that basin deepening was occurring in the Tally Pond Belt during the deposition of the Lemarchant deposit (Pollock, 2004; McNicoll et al., 2010; Lode et al., 2016a; Lode et al., 2017). We suggest that the Lemarchant deposit was situated around 1500 m depth during stages 1 and 2 of mineralization, allowing for boiling to occur at lower temperatures (150–275 °C) during stages 1 and 2 of mineralization (Butterfield et al., 1990; Hannington et al., 1995; Gill et al., 2016). However, progressive deepening of the basin below 1500 m would have interrupted boiling and prevented fluid-phase separation, and allowed the fluid to reach higher temperatures due to increasing pressure from the overlying water column (e.g., Butterfield et al., 1990). Correspondingly, hotter fluids could have leached Cu (at T > 300 °C; e.g., Lydon, 1988; Large, 1992; Ohmoto, 1996) resulting in the deposition of a chalcopyrite-bearing mineral assemblages found in stages 3 and 4 of mineralization. The sulphur isotope signatures from this assemblage are consistent with minimal influence from magmatic SO_2 and are dominated by TSR ± igneous leaching, which is consistent with the shift to deeper water hydrothermal activity, absence of fluid boiling, and regional models for the evolution of the Tally Pond group.

7. Conclusions

Radiogenic and stable isotope data from the precious metal bearing, polymetallic Lemarchant VMS deposit provide insight into the sources of metals and sulphur in the deposit. Regional- to deposit-scale Pb isotope data presented here is non-homogenous but consistent, and implies Pb isotopes derived from at least two different sources during formation of these VMS deposits. The observed trend in Lemarchant Pb isotopes intersects the young upper crust growth curve at ~500 Ma,

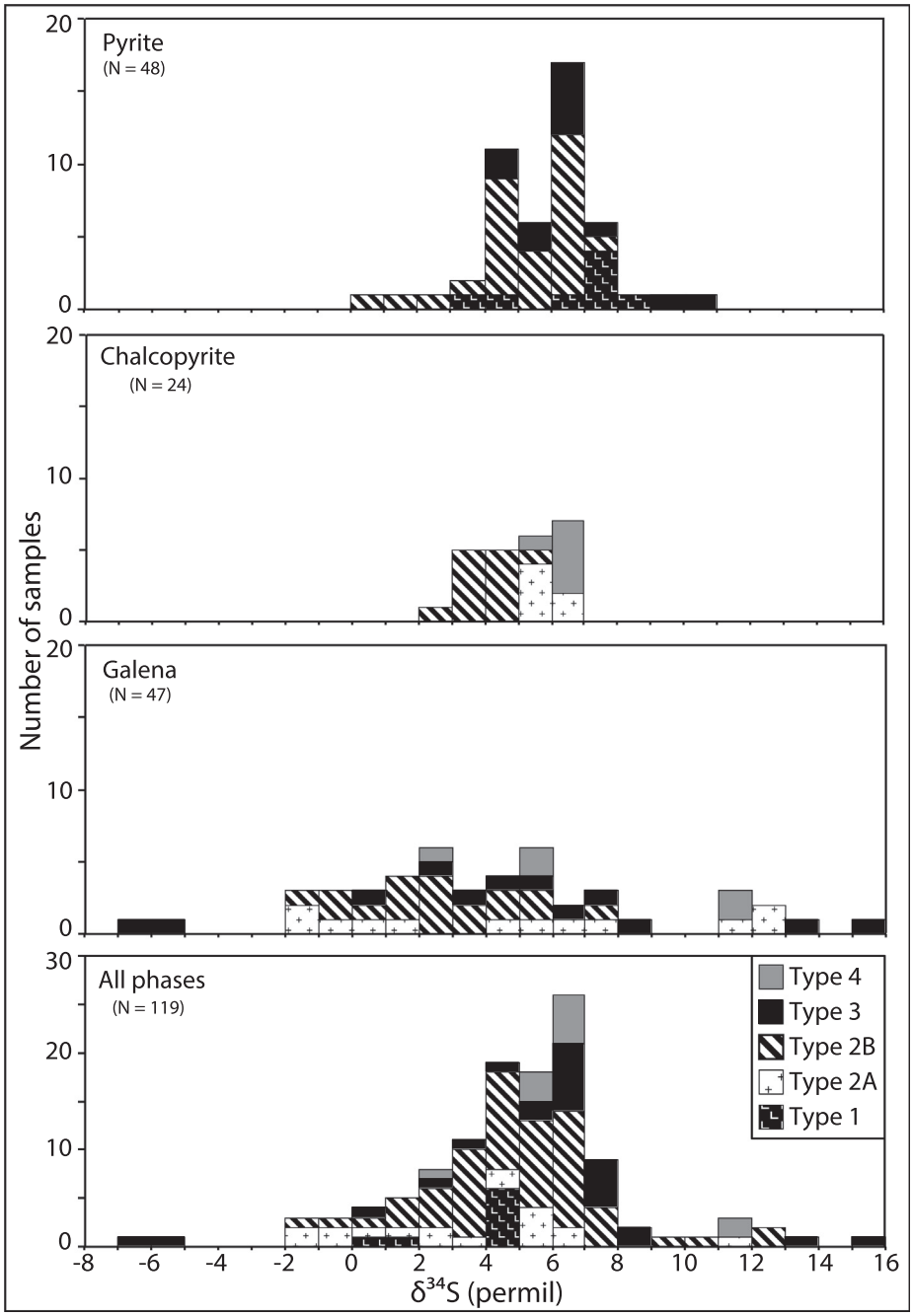

Fig. 7. Frequency distribution of $\delta^{34}S$ values in analyzed sulfides (pyrite, galena and chalcopyrite) from each of the five mineral assemblage types at the Lemarchant deposit.

suggesting a majority of Pb in the deposit originated from a young upper crust. This is consistent with regional tectonic models for the Tally Pond group, and with derivation of Pb from Neoproterozoic volcanic arc basement rocks in the region. However, the Lemarchant samples trend towards lower μ values that require additional input from more juvenile sources (i.e., basaltic material), which were either derived from more juvenile Neoproterozoic rocks, or from the underlying mafic rocks of the Tally Pond group.

Sulphur isotope ratios in sulphide minerals from Lemarchant evolve throughout the depositional history of the massive sulphide deposit, and suggest that H_2S may be derived from three main sources: (1) thermochemically reduced seawater sulphate ($\delta^{34}S > 0$); (2) igneous sulphide leached from basement rock ($\delta^{34}S \sim 0$); and (3) light H_2S derived from disproportionation of magmatic SO_2 ($\delta^{34}S < 0$). In the initial stages of mineralization (stages 1–2), and in particular stage 2, sulphide minerals have lighter $\delta^{34}S$ values that are consistent with a partial contribution of magmatic sulphur. The low $\delta^{34}S$ signatures are also associated with sulphosalt-rich mineral assemblages that contain epithermal suite trace element enrichments, bladed barite, and mineral textures that are commonly associated with magmatic-hydrothermal fluids and fluid boiling at lower temperatures on the shallow seafloor. The third and fourth stages of mineralization are characterized by mineral assemblages interpreted to have formed at higher temperatures (i.e., $T > 300\,^{\circ}C$) and in deeper water (> 1500 m water depth), and are associated with generally heavier $\delta^{34}S$ values in sulphide minerals that suggest boiling was prohibited. These latter stages of mineralization were likely predominated by sulphur derived from thermochemical sulphate reduction (TSR) of seawater sulphate and from leaching of

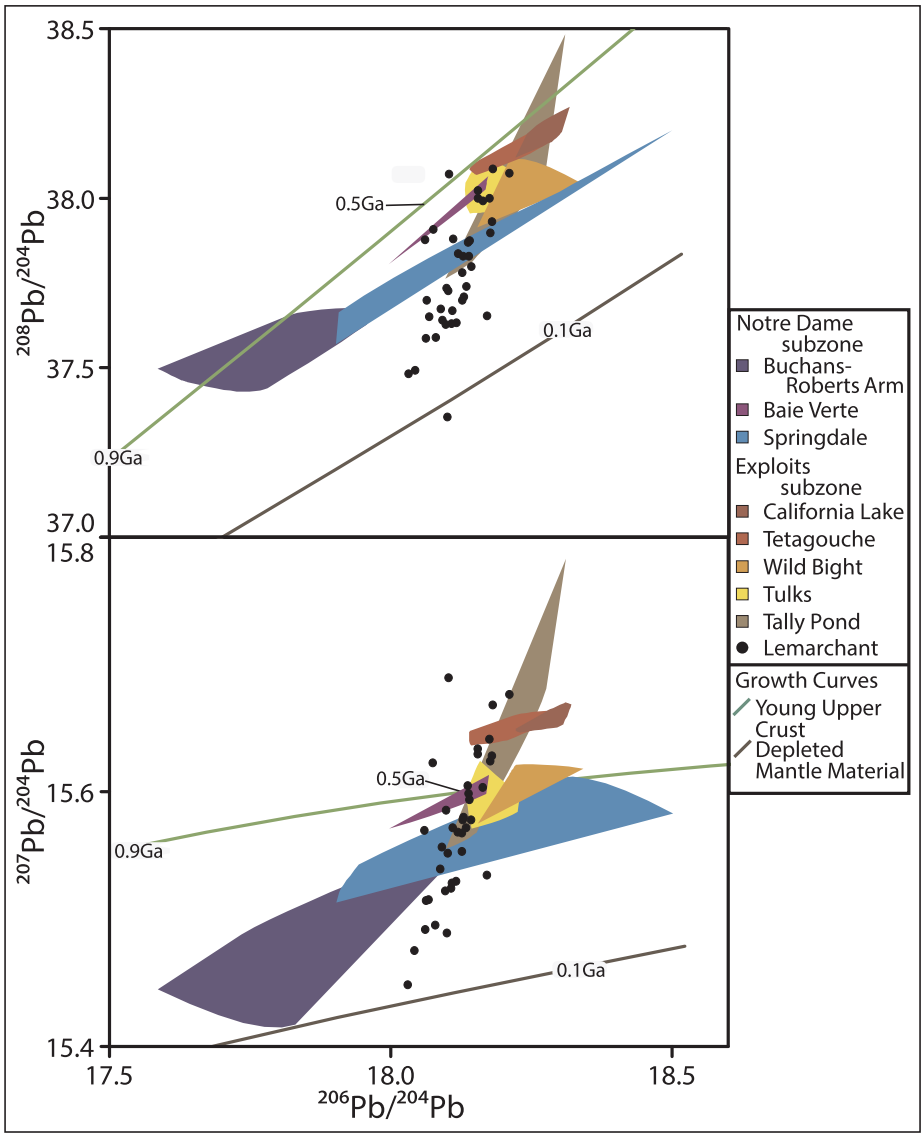

Fig. 8. Thorogenic and uranogenic lead isotope data for select Appalachian VMS deposits, including the Lemarchant deposit (outliers excluded). Data for the Springdale, Baie Verte and Buchans-Roberts Arm volcanic belts (Notre Dame subzone), and Tally Pond and Tulks volcanic belts, Wild Bight, California Lake and Tetagouche Groups (Exploits subzone) from Swinden and Thorpe (1984), Cumming and Krstic (1987), Winter and Wilton (2000), Pollock and Wilton (2001), Thorpe (2008), and Wilton (unpublished data). Growth curves for the young upper crust (green line) and depleted mantle material (brown line) (Kramers and Tolstikhin, 1997) shown for comparison. (For interpretation of the references to colour in this figure legend, the reader is referred to the web version of this article.)

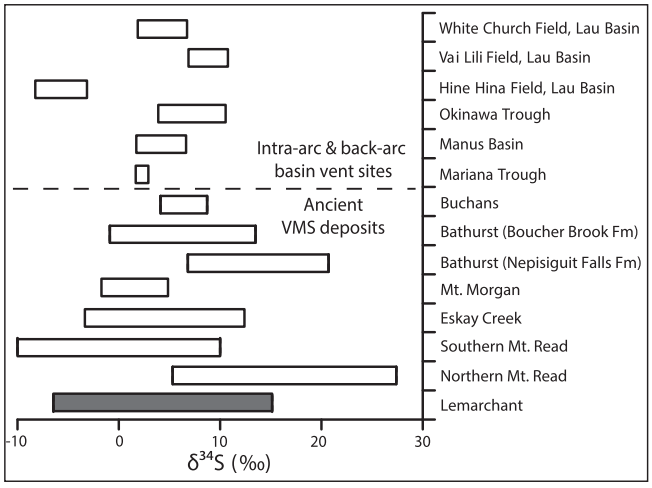

Fig. 9. Range of $\delta^{34}S$ values from Lemarchant, compared with $\delta^{34}S$ values from modern black smoker deposits (Lau Basin, Okinawa Trough, Manus Basin and Mariana Trough) and from ancient precious metal enriched VMS deposits in the Appalachians (Buchans, Bathurst) and globally (Eskay Creek, Mt. Morgan, Mt. Read volcanics) (data from Herzig et al., 1998; Huston, 1999 (does not include $\delta^{34}S$ values from galena); Sherlock et al., 1999; Ulrich et al., 2002).

igneous basement rocks. The radiogenic and stable isotope systematics of the Zn-Pb-Cu-Ag-Au Lemarchant deposit have implications for understanding the source(s) and deposition of base and precious metals in similar VMS deposits in the Appalachians and globally.

Acknowledgements

The GSC Targeted Geoscience Initiative 4 Program and the Research Affiliate Program of NRCan provide the majority of funding for this project. Grants to Dr. Stephen J. Piercey, including an NSERC Discovery Grant and the NSERC-Altius Industrial Research Chair in Mineral Deposits supported by Natural Sciences and Engineering Research Council of Canada (NSERC), Altius Resources Inc., and the Research and Development Corporation of Newfoundland and Labrador provide additional funding for this project. Access to the Lemarchant drill core was provided by the Canadian Zinc Corporation and the Paragon Minerals Corporation (a 100% owned subsidiary of Canadian Zinc Corporation). Research conducted at the MAF-IIC Facility derived support from the Core Research Equipment & Instrument Training Network (CREAIT) at the Memorial University of Newfoundland. Many thanks to Stefanie Lode, Jonathan Cloutier and Stefanie Brueckner for their technological help with the SIMS, and their guidance with the treatment and interpretation of Lemarchant Pb and S isotope data.

Earlier reviews of this manuscript by Aphrodite Indares and Jan Peter as part of an earlier MSc thesis evaluation are gratefully acknowledged. David Huston and Jim Franklin are thanked for their thorough and thoughtful reviews, which have greatly improved this manuscript.

Appendix A. Supplementary data

Supplementary data to this article can be found online at https://doi.org/10.1016/j.oregeorev.2018.11.008.

References

Brueckner, S.M., Piercey, S.J., Layne, G.D., Piercey, G., Sylvester, P.J., 2015. Variations of sulfur isotope signatures in sulfides from the metamorphosed Cu(-Au) volcanogenic massive sulfide Ming deposit, Newfoundland Appalachians. Mineral. Deposita 50 (5), 619–640.

Butterfield, D.A., Massoth, G.J., McDuff, R.E., Lupton, J.E., Lilley, M.D., 1990. Geochemistry of hydrothermal fluids from Axial Seamount hydrothermal emissions study vent field, Juan de Fuca Ridge: Subseafloor boiling and subsequent fluid-rock interaction. J. Geophys. Res. 95 (B8), 12895–12921.

Canfield, D.E., 2004. The evolution of the Earth surface sulphur reservoir. Am. J. Sci. 304, 839–861.

Chiaradia, M., Tripodi, D., Fontboté, L., Reza, B., 2008. Geologic setting, mineralogy, and geochemistry of the early Tertiary Au-rich volcanic-hosted massive sulphide deposit of La Plata, Western Cordillera. Ecuador. Econ. Geol. 103, 161–183.

Claypool, G.E., Holser, W.T., Kaplan, I.R., Sakai, H., Zak, I., 1980. The age curves of sulphur and oxygen isotopes in marine sulphate and their mutual interpretation. Chem. Geol. 28, 199–260.

Cloutier, J., Piercey, S.J., Layne, G.D., Heslop, J., Hussey, A., Piercey, G., 2015. Styles, textural evolution and sulfur isotope systematics of Cu-rich sulfides from the Cambrian Whalesback Volcanogenic Massive Sulfide (VMS), deposit, central Newfoundland. Canada. Econ. Geol. 110, 1215–1234.

Copeland, D.A., McCleneghan, S.M., Piercey, S.J., 2008. Ninth year assessment report on diamond drilling, lithogeochemistry, pulse EM surveying and linecutting on license 8183M, South Tally Pond Property, Rogerson Lake area, Newfoundland and Labrador NTS 12A/10 and 12A/07. Newfoundland and Labrador Geological Survey. Assessment Report prepared for Paragon Minerals Corp. and Altius Minerals Corp. 91 p.

Cumming, G.L., Krstic, D., 1987. Detailed lead isotope study of Buchans and related ores. In: Kirkham, R.V. (Ed.), Buchans Geology. Newfoundland, Geological Survey of Canada, pp. 227–234 Paper 86-24, Report 13.

de Ronde, C.E.J., 1995. Fluid chemistry and isotopic characteristics of seafloor hydrothermal systems and associated VMS deposits: potential for magmatic contributions. In: Mineralogical Association of Canada Short Course Series 23. pp. 479–509.

de Ronde, C.E.J., Hannington, M.D., Stoffers, P., Wright, I.C., Ditchburn, R.G., Reyes, A.G., Baker, E.T., Massoth, G.J., Lupton, J.E., Walker, S.L., Greene, R.R., Soong, C.W.R., Ishibashi, J., Lebon, G.T., Bray, C.J., Resing, J.A., 2005. Evolution of a submarine magmatic-hydrothermal system: Brothers Volcano, Southern Kermadec Arc, New Zealand. Econ. Geol. 100, 1097–1133.

Dube, B., Gosselin, P., Mercier-Langevin, P., Hannington, M., Galley, A., 2007. Gold-rich volcanogenic massive sulphide deposits. In: Goodfellow, W.D. (Ed.), Mineral Deposits of Canada: A Synthesis of Major Deposit-types, District Metallogeny, the Evolution of Geological Provinces, and Exploration Methods. Geological Association of Canada, pp. 75–94 Mineral Deposits Division, Special Publication 5.

Dunning, G.R., Swinden, H.S., Kean, B.F., Evans, D.T.W., Jenner, G.A., 1991. A Cambrian island arc in Iapetus; geochronology and geochemistry of the Lake Ambrose volcanic belt, Newfoundland Appalachians. Geol. Mag. 128, 1–17.

Evans, D., Kean, B., 2002. The Victoria Lake Supergroup, Central Newfoundland – Its Definition, Setting and Volcanogenic Massive Sulphide Mineralization. Newfoundland Department of Mines and Energy Geological Survey, Open File NFLD/2790, 68 p.

Fouquet, Y., Marcoux, E., 1995. Lead isotope systematics in Pacific hydrothermal sulphide deposits. J. Geophys. Res. 100, 6025–6040.

Franklin, J., Gibson, H., Jonasson, I., Galley, A., 2005. Volcanogenic massive sulphides. Economic Geology 100th Anniversary Volume, pp. 523–560.

Fraser, D., Giroux, G.H., Copeland, D.A., Devine, C.A., 2012. Technical report and resource minerals estimate on the Lemarchant deposit, South Tally Pond VMS project, Central Newfoundland, Canada. NI 43-101 Technical Report prepared for Paragon Minerals Corp. 132 p.

Galley, A., Hannington, M., Jonasson, I., 2007. Volcanogenic massive sulphide deposits. In: Goodfellow, W.D. (Ed.), Mineral Deposits of Canada: A Synthesis of Major Deposit-types, District Metallogeny, the Evolution of Geological Provinces, and exploration methods. Geological Association of Canada, pp. 141–161 Mineral Deposits Division, Special Publication 5.

Gibson, H.L., Allen, R.L., Riverin, G., Lane, T.E., 2007. The VMS model; advances and application to exploration. In: Abstracts, Decennial International Conference on Mineral Exploration 5, pp. 713–730.

Gill, S.B., Piercey, S.J., 2014. Styles of Mineralization and Sulphide Mineral Zonation in the Cambrian Zn-Pb-Cu-Ag-Au Lemarchant Volcanogenic Massive Sulphide (VMS) deposit, Newfoundland and Labrador – Preliminary Observations. Geological Survey of Canada, pp. 17 Current Research 2014-05.

Gill, S.B., Piercey, S.J., Layton-Matthews, D., Layne, G.D., Piercey, G., 2015. Mineralogical, sulphur, and lead isotopic study of the Lemarchant Zn-Pb-Cu-Ag-Au-VMS deposit: Implications for precious-metal enrichment processes in the VMS environment. In: Peter, J.M., Mercier-Langevin, P. (Eds.), Targeted Geoscience Initiative 4: Contributions to the Understanding of Volcanogenic Massive Sulphide Deposit Genesis and Exploration Methods Development. Geological Survey of Canada, pp. 183–195 Open File 7853.

Gill, S.B., Piercey, S.J., Layton-Matthews, D., 2016. Mineralogy and metal zoning of the Cambrian Zn-Pb-Cu-Ag-Au Lemarchant volcanogenic massive sulphide (VMS) deposit, Newfoundland. Can. Mineral. 54, 1307–1344.

Goodfellow, W.D., Peter, J.M., 1996. Sulphur isotope composition of the Brunswick No. 12 massive sulphide deposit, Bathurst Mining Camp, New Brunswick: implications for ambient environment, sulphur source, and ore genesis. Can. J. Earth Sci. 33, 231–251.

Goodfellow, W.D., 2007. Metallogeny of the Bathurst Mining Camp, northern New Brunswick. In: Goodfellow, W.D. (Ed.), Mineral Deposits of Canada: A Synthesis of Major Deposit-types, District Metallogeny, the Evolution of Geological Provinces, and Exploration Methods. Geological Association of Canada, pp. 449–469 Mineral Deposits Division, Special Publication 5.

Halbach, P., Nakamura, K.-I., Wahsner, M., Lange, J., Sakai, H., Kaeselitz, L., Hansen, R.D., Yamano, M., Post, J., Prause, B., Seifert, R., Michaelis, W., Teichmann, F., Kinoshita, M., Maerten, A., Ishibashi, J., Czerwinski, S., Blum, N., 1989. Probable modern analogue of Kuroko-type massive sulphide deposits in the Okinawa Trough back-arc basin. Nature 338, 496–499.

Hannington, M.D., Poulsen, K.H., Thompson, J.F.H., Sillitoe, R.H., 1999a. Volcanogenic gold in the massive sulfide environment. Rev. Econ. Geol. 8, 325–356.

Hannington, M., Monecke, T., 2009. Modern submarine hydrothermal systems – a global perspective on distribution, size and tectonic settings. In: Cousens, B., Piercey, S.J. (Eds.), Submarine Volcanism and Mineralization: Modern through Ancient. Geological Association of Canada, pp. 91–146 Mineral Deposits Division, Short Course Notes 19.

Hannington, M.D., Jonasson, I.R., Herzig, P.M., Petersen, S., 1995. Physical and chemical processes of seafloor mineralization at mid-ocean ridges. In: Humphris, S.E., Zierenberg, R.A., Mullineaux, L.S., Thomson, R.E. (Eds.), Seafloor Hydrothermal Systems: Physical, Chemical, Biological, and Geological Interactions. American Geophysical Union, pp. 115–157 Geophysical Monograph Series 91.

Hannington, M.D., Poulsen, K.H., Thompson, J.F.H., Sillitoe, R.H., 1999b. Volcanogenic gold in the massive sulphide environment. Rev. Econ. Geol. 8, 325–356.

Herzig, P.M., Hannington, M.D., Fouquet, Y., von Stackelberg, U., Petersen, S., 1993. Gold-rich polymetallic sulphides from the Lau back arc and implications for the geochemistry of gold in sea-floor hydrothermal systems of the Southwest Pacific. Econ. Geol. 88, 2182–2209.

Herzig, P., Hannington, M., Arribas Jr, A., 1998. Sulphur isotopic composition of hydrothermal precipitates from the Lau back-arc: implications for magmatic contributions to seafloor hydrothermal systems. Mineral. Deposita 33, 226–237.

Huston, D.L., 1999. Stable isotopes and their significance for understanding the genesis of volcanic-hosted massive sulphide deposits: a review. Rev. Econ. Geol. 8, 157–179.

Huston, D.L., 2000. Gold in volcanic-hosted massive sulphide deposits; distribution, genesis, and exploration. Rev. Econ. Geol. 13, 401–426.

Huston, D.L., Relvas, J.M.R.S., Gemmell, J.B., Drieberg, S., 2011. The role of granites in volcanic-hosted massive sulphide ore-forming systems: an assessment of magmatic–hydrothermal contributions. Mineral. Deposita 46, 473–507.

Janecky, D.R., Shanks, W.C., 1988. Computational modeling of chemical and sulphur isotopic reaction processes in sea-floor hydrothermal systems; chimneys, massive sulphide, and subjacent alteration zones. Can. Mineral. 26, 805–825.

Jensen, M.L., 1967. Sulphur isotopes and mineral genesis. In: Barnes, H.L. (Ed.), Geochemistry of Hydrothermal Ore Deposits. Rinehart and Winston, New York, pp. 143–165.

Kampschulte, A., Strauss, H., 2004. The sulphur isotopic evolution of Phanerozoic seawater based on the analysis of structurally substituted sulphate in carbonates. Chem. Geol. 204, 255–286.

Kramers, J.D., Tolstikhin, I.N., 1997. Two terrestrial lead isotope paradoxes, forward transport modeling, core formation and the history of the continental crust. Chem. Geol. 139, 75–110.

Lajoie, M.-E., 2017. Genesis of Barite Associated with the Lemarchant Zn-Pb-Cu-Ag-Au-Rich Volcanogenic Massive Sulfide (VMS) deposit: Implications for the Genesis of VMS-related Barite, Cambrian Seawater Chemistry, and the Origin of Barite-rich VMS Deposits. Unpublished M.Sc. thesis. Memorial University of Newfoundland, St. John's, Newfoundland, Canada, pp. 300.

Large, R., 1992. Australian volcanic-hosted massive sulfide deposits: features, styles, and genetic models. Econ. Geol. 87, 471–510.

Lajoie, M.-E., Piercey, S.J., Conliffe, J., Layton-Matthews, D., submitted for publication. Geology, mineralogy, S and Sr isotope geochemistry, and fluid inclusion analysis of barite associated with the Lemarchant Zn-Pb-Cu-Ag-Au-rich volcanogenic massive sulphide (VMS) deposit, Newfoundland, Canada: implications for the genesis of VMS-related barite. Can. J. Earth Sci.

Lode, S., Piercey, S.J., Devine, C.A., 2015. Geology, mineralogy, and lithogeochemistry of metalliferous mudstones associated with the Lemarchant volcanogenic massive sulphide deposit, Tally Pond Belt, Central Newfoundland. Econ. Geol. 110, 1835–1859.

Lode, S., Piercey, S.J., Squires, G.D., 2016a. Role of metalliferous mudstones and graphitic shales in the localization, genesis, and paleo-environment of volcanogenic massive sulphide deposits of the Tally Pond volcanic belt, central Newfoundland, Canada. Can. J. Earth Sci.

Lode, S., Piercey, S.J., Layne, G.D., Piercey, G., 2016b. Multiple sulphur and lead sources recorded in hydrothermal exhalites associated with the Lemarchant volcanogenic massive sulphide deposit, central Newfoundland, Canada. Mineral Deposita.

Lode, S., Piercey, S.J., Cloutier, C., 2017. Provenance of exhalites associated with the

Lemarchant volcanogenic massive sulphide (VMS) deposit, central Newfoundland, Canada: insights from Nd isotopes and lithogeochemistry. J. Geol. Soc. London. 174, 954–967.
Lydon, J.W., 1988. Volcanogenic Massive Sulphide Deposits, Part 2: Genetic Models. Geological Association of Canada, Geoscience Canada, pp. 155–181.
Marini, L., Moretti, R., Accornero, M., 2011. Sulphur isotopes in magmatic-hydrothermal systems, melts, and magmas. Rev. Mineral. Geochem. 73, 423–492.
McGill, R., Tukey, J.W., Larsen, W.A., 1978. Variations of box plots. Am. Stat. 32, 12–16.
McNicoll, V., Squires, G., Kerr, A., Moore, P., 2010. The Duck Pond and Boundary Cu-Zn deposits, Newfoundland; new insights into the ages of host rocks and the timing of VHMS mineralization. Can. J. Earth Sci. 47, 1481–1506.
Mortensen, J.K., Dusel-Bacon, C., Hunt, J., Gabites, J., 2006. Lead isotopic constraints on the metallogeny of middle and late Paleozoic syngenetic base metal occurrences in the Yukon-Tanana and Slide Mountain/Seventymile terranes and adjacent portions of the North American miogeocline. In: Colpron, M., Nelson, J.L. (Eds.), Paleozoic Evolution and Metallogeny of Pericratonic Terranes at the Ancient Pacific Margin of North America, Canadian and Alaskan Cordillera. Geological Association of Canada, pp. 261–279 Special Paper 45.
Ohmoto, H., 1972. Systematics of sulphur and carbon isotopes in hydrothermal ore deposits. Econ. Geol. 67, 551–578.
Ohmoto, H., 1996. Formation of volcanogenic massive sulphide deposits; the Kuroko perspective. Ore Geol. Rev. 10, 135–177.
Ohmoto, H., Rye, R., 1979. Isotopes of sulphur and carbon. In: Barnes, H.L. (Ed.), Geochemistry of Hydrothermal Ore Deposits, second ed. John Wiley & Sons, New York, pp. 509–567.
Ohmoto, H., Lasaga, A.C., 1982. Kinetics of reactions between aqueous sulphates and sulphides in hydrothermal systems. Geochim. Cosmochim. Acta 46, 1727–1745.
Ohmoto, H., Goldhaber, M.B., 1997. Sulphur and carbon isotopes. In: Barnes, H.L. (Ed.), Geochemistry of Hydrothermal Ore Deposits, third ed. John Wiley & Sons, New York, pp. 517–611.
Paytan, A., Gray, E.T., 2012. Sulphur isotope stratigraphy. In: Gradstein, F.M., Ogg, J.G., Schmitz, M., Ogg, G. (Eds.), The Geologic Timescale 2012. Elsevier, Amsterdam, pp. 167–180.
Piercey, S.J., Hinchey, J., 2012. Volcanogenic massive sulphide (VMS) deposits of the Central Mineral Belt, Newfoundland. Geological Association of Canada–Mineralogical Association of Canada Joint Annual Meeting, Field Trip Guidebook B, Newfoundland and Labrador Department of Natural Resources, Geological Survey, Open File NFLD/3173, 56 pp.
Piercey, S.J., Squires, G.C., Brace, T.D., 2014. Lithostratigraphic, hydrothermal, and tectonic setting of the Boundary volcanogenic massive sulphide deposit, Newfoundland Appalachians, Canada: formation by subseafloor replacement in a Cambrian rifted arc. Econ. Geol. 109, 661–687.
Pollock, J., Wilton, D., 2001. Metallogenic Studies of the Tally Pond Belt, Victoria Lake Group: Trace Element Geochemistry and Lead Isotope Data from the Exploits Subzone, Newfoundland. Newfoundland and Labrador Department of Natural Resources, pp. 247–266 Geological Survey, Current Research 2001-01.
Pollock, J., 2004. Geology and Paleotectonic History of the Tally Pond Group, Dunnage Zone, Newfoundland Appalachians: An Integrated Geochemical, Geochronological, Metallogenic and Isotopic Study of a Cambrian Island Arc Along the Peri-Gondwanan Margin of Iapetus. Unpublished M.Sc. thesis. Memorial University of Newfoundland, St. John's, Newfoundland, Canada, pp. 420.
Rogers, N., van Staal, C., 2002. Toward a Victoria Lake Supergroup: A Provisional Stratigraphic Revision of the Red Indian to Victoria Lakes Area, central Newfoundland. Newfoundland Department of Mines and Energy, pp. 185–195 Geological Survey, Current Research Report 2002-01.
Rogers, N., van Staal, C.R., McNicoll, V., Pollock, J., Zagorevski, A., Whalen, J., 2006. Neoproterozoic and Cambrian arc magmatism along the eastern margin of the Victoria Lake supergroup: a remnant of Ganderian basement in central Newfoundland? Precambrian Res. 147, 320–341.
Roth, T., Thompson, J.F.H., Barrett, T.J., 1999. The precious metal-rich Eskay Creek Deposit, northwestern British Columbia. Rev. Econ. Geol. 8, 357–373.
Rye, R.O., 1993. The evolution of magmatic fluids in the epithermal environment; the stable isotope perspective. Econ. Geol. 88, 733–752.
Sakai, H., Dickson, F., 1978. Experimental determination of the rate and equilibrium fractionation factors of sulphur isotope exchange between sulphate and sulphide in slightly acid solutions at 300 C and 1000 bars. Earth Planet. Sci. Lett. 39, 151–161.
Sakai, H., Des Marais, D., Ueda, A., Moore, J., 1984. Concentrations and isotope ratios of carbon, nitrogen and sulphur in ocean-floor basalts. Geochim. Cosmochim. Acta 48, 2433–2441.
Sato, K., Delevaux, M.H., Doe, B.R., 1981. Lead isotope measurements on ores, igneous and sedimentary rocks from the Kuroko mineralization area. Geochem. J. 15, 135–140.
Seal, R.R., 2006. Sulphur isotope geochemistry of sulphide minerals. Rev. Mineral. Geochem. 61, 633–677.
Seyfried, W.E., Bischoff, J.L., 1981. Experimental seawater-basalt interaction at 300°C, 500 bars, chemical exchange, secondary mineral formation and implications for the transport of heavy metals. Geochim. Cosmochim. Acta 45, 135–149.
Shanks, W., 2001. Stable isotopes in seafloor hydrothermal systems: vent fluids, hydrothermal deposits, hydrothermal alteration, and microbial processes. Rev. Mineral. Geochem. 43, 469–525.
Shanks, W., Böhlke, J.K., Seal, R.R., 1995. Stable isotopes in mid-ocean ridge hydrothermal systems: interactions between fluids, minerals, and organisms. In: Humphris, S.E., Zierenberg, R.A., Mullineaux, L.S., Thomson, R.E. (Eds.), Seafloor Hydrothermal Systems: Physical, Chemical, Biological, and Geological Interactions. American Geophysical Union, pp. 194–221 Geophysical Monograph 91.
Sillitoe, R.H., Hannington, M.D., Thompson, J.F.H., 1996. High sulfidation deposits in the volcanogenic massive sulphide environment. Econ. Geol. 91, 204–212.
Sherlock, R.L., Roth, T., Spooner, E.T.C., Bray, C.J., 1999. Origin of the Eskay Creek precious metal-rich volcanogenic massive sulphide deposit; fluid inclusion and stable isotope evidence. Econ. Geol. 94, 803–824.
Squires, G., Moore, P., 2004. Volcanogenic Massive Sulphide Environments of the Tally Pool Volcanics and Adjacent Area; Geological, Lithogeochemical and Geochronological Results. Geological Survey, Current Research Report 2004-01. Newfoundland Department of Mines and Energy, pp. 63–91.
Stacey, J.S., Kramers, J., 1975. Approximation of terrestrial lead isotope evolution by a two-stage model. Earth Planet. Sci. Lett. 26, 207–221.
Swinden, H.S., Thorpe, R., 1984. Variations in style of volcanism and massive sulphide deposition in Early to Middle Ordovician island-arc sequences of the Newfoundland Central Mobile Belt. Econ. Geol. 79, 1596–1619.
Swinden, H., Kean, B., Dunning, G., 1988. Geological and paleotectonic settings of volcanogenic massive sulphide mineralization in Central Newfoundland. In: The Volcanogenic Sulphide Districts of Newfoundland. Geological Association of Canada, Mineral Deposits Division, pp. 2–27.
Thorpe, R.I., 1999. The Pb isotope linear array for volcanogenic massive sulfide deposits of the Abitibi and Waawa Subprovinces, Canadian Shield. Econ. Geol. Monograph 10, 555–575.
Thorpe, R.I., 2008. Release of Lead Isotope Data in 4 Databases; Canadian, Western Superior, Foreign, and Whole Rock and Feldspar. Geological Survey of Canada, pp. 42 Open File Report 5664.
Tosdal, R., Wooden, J., Bouse, R., 1999. Pb isotopes, ore deposits, and metallogenic terranes: Application of radiogenic isotopes to ore deposit research and exploration. Rev. Econ. Geol. 12, 1–28.
Ueda, A., Sakai, H., 1984. Sulphur isotope study of Quaternary volcanic rocks from the Japanese Islands Arc. Geochim. Cosmochim. Acta 48, 1837–1848.
Ulrich, T., Golding, S.D., Kamber, B.S., Khin, Z., Taube, A., 2002. Different mineralization styles in a volcanic-hosted ore deposit: the fluid and isotopic signatures of the Mt Morgan Au–Cu deposit, Australia. Ore Geol. Rev. 22, 61–90.
van Staal, C., Barr, S., 2012. Lithospheric architecture and tectonic evolution of the Canadian Appalachians and associated Atlantic margin. In: Percival, J.A., Cook, F.A., Clowes, R.M. (Eds.), Tectonic Styles in Canada Revisited: the Lithoprobe Perspective. Geological Association of Canada, pp. 41–95 Special Paper 49, Chapter 2.
White, N.C., Hedenquist, J.W., 1990. Epithermal environments and styles of mineralization: Variations and their causes, and guidelines for exploration. J. Geochem. Expl. 36, 445–474.
Williams, H., Colman-Sadd, S.P., Swinden, H.S., 1988. Tectonic-stratigraphic Subdivisions of Central Newfoundland. Geological Survey of Canada, pp. 91–98 Current Research Part B 1988-01.
Winter, L.S., Wilton, D.H.C., 2000. New lithogeochemical and Pb isotope data from Buchans area, central Newfoundland. Atl. Geol. 36, 176.
Zagorevski, A., Van Staal, C.R., McNicoll, V., Rogers, N., 2007. Upper Cambrian to upper Ordovician peri-Gondwanan island arc activity in the Victoria Lake supergroup, Central Newfoundland: tectonic development of the northern Ganderian margin. Am. J. Sci. 307, 339–370.
Zartman, R., Doe, B., 1981. Plumbotectonics—the model. Tectonophysics 75, 135–162.